DTNSRDC-80/124

AD A092725

DAVID W. TAYLOR NAVAL SHIP RESEARCH AND DEVELOPMENT CENTER

Bethesda, Maryland 20084

LEVEL II

VORTEX SHEDDING FROM FINNED CIRCULAR CYLINDERS

by

John G. Telste
Hans J. Lugt

APPROVED FOR PUBLIC RELEASE: DISTRIBUTION UNLIMITED

COMPUTATION, MATHEMATICS, AND LOGISTICS DEPARTMENT
RESEARCH AND DEVELOPMENT REPORT

DTNSRDC-80/124

VORTEX SHEDDING FROM FINNED CIRCULAR CYLINDERS

MAJOR DTNSRDC ORGANIZATIONAL COMPONENTS

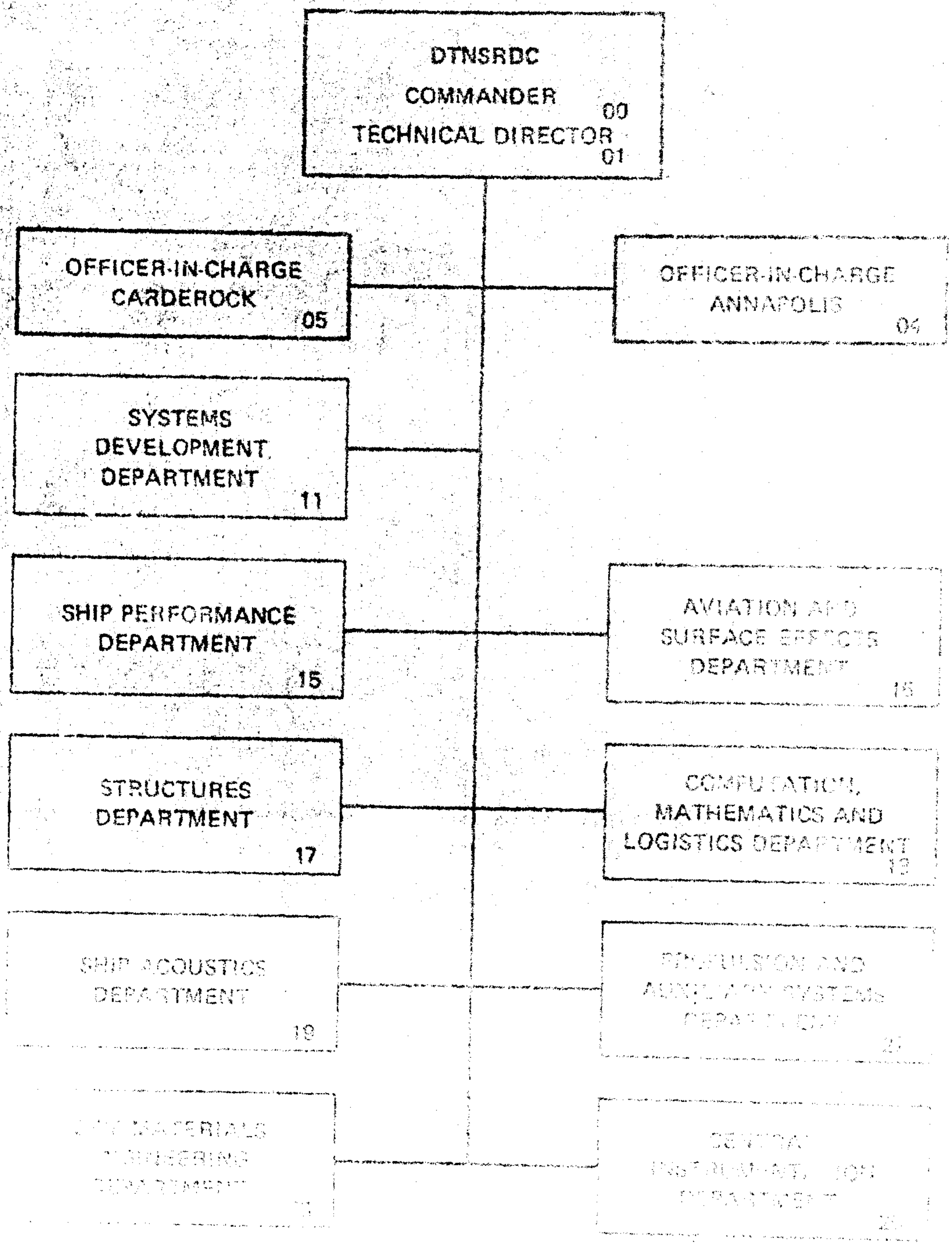

REPORT DOCUMENTATION PAGE

READ INSTRUCTIONS BEFORE COMPLETING FORM

1. REPORT NUMBER: DTNSRDC-80/124
2. GOVT ACCESSION NO.: AD-A092 725
3. RECIPIENT'S CATALOG NUMBER:
4. TITLE (and Subtitle): VORTEX SHEDDING FROM FINNED CIRCULAR CYLINDERS
5. TYPE OF REPORT & PERIOD COVERED: Final
6. PERFORMING ORG. REPORT NUMBER:
7. AUTHOR(s): John G. Telste [redacted] Hans J. Lugt
8. CONTRACT OR GRANT NUMBER(s): SR 01402
9. PERFORMING ORGANIZATION NAME AND ADDRESS: David W. Taylor Naval Ship Research and Development Center, Bethesda, Maryland 20084
10. PROGRAM ELEMENT, PROJECT, TASK AREA & WORK UNIT NUMBERS: (See reverse side)
11. CONTROLLING OFFICE NAME AND ADDRESS:
12. REPORT DATE: Nov[redacted]80
13. NUMBER OF PAGES: 49 (12) 52
14. MONITORING AGENCY NAME & ADDRESS (if different from Controlling Office):
15. SECURITY CLASS. (of this report): UNCLASSIFIED
15a. DECLASSIFICATION/DOWNGRADING SCHEDULE:
16. DISTRIBUTION STATEMENT (of this Report):

APPROVED FOR PUBLIC RELEASE: DISTRIBUTION UNLIMITED

17. DISTRIBUTION STATEMENT (of the abstract entered in Block 20, if different from Report):
18. SUPPLEMENTARY NOTES:
19. KEY WORDS (Continue on reverse side if necessary and identify by block number)

Vortex shedding
Finned bodies
Conformal mapping
Point vortices

20. ABSTRACT (Continue on reverse side if necessary and identify by block number)

A computer program has been developed to simulate vortex shedding from circular cylinders with evenly distributed fins. These bodies may rotate continuously or oscillate in a parallel stream. The two-dimensional flow model consists of point vortices inserted in an otherwise potential-flow field. For the roll-up of the line of vortices the rediscretization scheme by Fink and Soh is used. Sample results are presented for vortex shedding from a flat plate at angles of attack of 45° and 90°, and from a circular cylinder with two fins at an angle of attack of 45°.

(Block 10)

Program Element 61152N
Task Area ZR0140201
Work Unit 1843-050
Program Element 61153N
Task Area SR0140301
Work Unit 1808-010

Accession For	
NTIS GRA&I	X
DDC TAB	
Unannounced	
Justification	
By	
Distribution/	
Availability Codes	
Dist.	Avail and/or special
A	

TABLE OF CONTENTS

LIST OF FIGURES

LIST OF TABLES

NOTATION

a	Radius of cylinder in z-plane
a_q	Coefficient in Laurent series (B1)
b	Distance from body center to fin tip
b_q	Coefficient in Laurent Series (B2)
B	Function in Equation (13)
B_1	Function in Equation (14)
c	Radius of circle in ζ-plane
k	Coefficient in Equation (4)
K_i	Total strength of the point vortices behind the i^{th} fin
ℓ	Coefficients in Equations (5) and (9)
m	Total number of point vortices in the field
M	Number of point vortices representing a single discontinuity line
n	Number of fins
p,q	Coefficients in Equation (7)
r,ϕ	Polar coordinates (r also coefficient in Equation (5))
Re	Reynolds number = $2bU/\nu$
s_k	Distance along discontinuity line of k^{th} point vortex from first point vortex in the line
s	Coefficient in Equation (6)
$\Delta\hat{s}$	Segment length of discontinuity line after rediscretization
S	Length of discontinuity line
t	Time
t_1,t_2	Coefficients in Equation (9)
u,v	Velocity components
U	Constant velocity of the parallel flow
w	Complex potential
w_p	Contribution to w from parallel flow
w_R	Contribution to w from rotation
w_V	Contribution to w from vortices
W	Constant velocity component in the Z-direction
x,y	Cartesian coordinates in z-plane

z	$= x + iy$
$\bar{z}$	$= x - iy$
z_1, z_2, z_3	Auxiliary planes
Z	Coordinate perpendicular to the x,y-plane
α	Angle of attack
β	Angle between line extending from the fin and line between tip and first vortex
γ	Strength density of discontinuity line
Γ	Gamma function
ζ	$= \xi + i\eta$
$\bar{\zeta}$	$= \xi - i\eta$
ξ, η	Cartesian coordinates in ζ-plane
Θ	Dihedral angle in Figure 2; also $\sigma = ce^{i\Theta}$
κ	Strength of vortex
ν	Kinematic viscosity
σ	Point on the circle in the ζ-plane
τ_1, τ_2	Coefficients in Equation (9)
ϕ, r	Polar coordinates
Φ	Potential function
ψ	Stream function
ω	Angular velocity

Subscripts:

0	Initial state
i	i^{th} fin
k	k^{th} point vortex
q	q^{th} coefficient in Laurent series

PREFACE

This report is part of a continuing effort at the Computation, Mathematics, and Logistics Department, with support from IR-inhouse funds and the 6.1 NAVSEA Mathematical Science Program, to study vortex shedding from solid bodies in a fluid flow and to apply the results to Navy problems. For the last ten years the major objective of this effort has been to investigate vortex generation and shedding in real fluids by the numerical solution of the Navier-Stokes equations. These successful studies, which resulted in numerous publications in the open literature, were originally restricted to moderate Reynolds-number flows about simply-shaped bodies. Today two-dimensional flows around bodies of quite arbitrary shape can be handled, but the solution of the Navier-Stokes equations for high Reynolds numbers still cannot be obtained. Instead, ideal fluid flow models with their well-known shortcomings must be used. This report describes one of two preliminary studies to develop a computer program for vortex shedding past arbitrarily shaped cylindrical bodies within the realm of ideal-fluid models. This report deals with vortex shedding from finned cylinders, and the forthcoming second report by R. Shoaff will address vortex shedding from arbitrarily shaped bodies excluding fins and other sharp protuberances. These purely two-dimensional flows then may be used in a strip theory to include at least some aspects of three-dimensional flows. The ultimate goal will be a computer code for vortex shedding from three-dimensional bodies.

ABSTRACT

A computer program has been developed to simulate vortex shedding from circular cylinders with evenly distributed fins. These bodies may rotate continuously or oscillate in a parallel stream. The two-dimensional flow model consists of point vortices inserted in an otherwise potential-flow field. For the roll-up of the line of vortices the rediscretization scheme by Fink and Soh is used. Sample results are presented for vortex shedding from a flat plate at angles of attack of 45° and 90°, and from a circular cylinder with two fins at an angle of attack of 45°.

ADMINISTRATIVE INFORMATION

The work presented in this report was supported by the Independent Research Program at the David W. Taylor Naval Ship Research and Development Center under Work Unit 1843-050, and the 6.1 NAVSEA Mathematical Sciences Program under Work Unit 1808-010.

1. INTRODUCTION

The simulation of vortex shedding from bodies in potential flow by means of point-vortex models has attracted the attention of many researchers in the last decade for a number of reasons. Persisting difficulties in solving the Navier-Stokes equations for large Reynolds numbers, the availability of large computers, and progress in the study of rolled-up discontinuity sheets have fostered the use of point-vortex models. The extensive literature on this subject includes recent survey papers by Fink and Soh,[1]* Saffman and Baker,[2] Clements and Maull,[3] Kato,[4] and Leonard.[5]

Although the neglect of viscosity limits the usefulness of point-vortex methods, in many cases details of the flow field can be obtained and a fairly good estimate of the force coefficients can be made.

This report presents the equations of motion for incompressible fluid flows past abruptly started circular cylinders with n evenly distributed fins of equal length. These cylinders may rotate continuously or they may oscillate. Some cases can be extended to elliptic cylinders. Point vortices are introduced into the potential flow around such cylinders to simulate the development and shedding of

---

*A complete listing of references is given on page 39.

vortices at the fins. A fixed interval of time elapses between successive introductions of point vortices. The computer program is checked for simple cases by comparing its results with solutions from the literature. Results for force coefficients and complicated flow problems of practical interest will be presented at a later time in another paper.

The formulas derived in this report and the computer program described here can be applied in missile aerodynamics and ship hydrodynamics. In particular, cross flows past cruciform fin configurations and past underwater vehicles with sails, rudders, stabilizers, bilge keels, and cables can be determined.

2. CONFORMAL TRANSFORMATIONS

For the computation of the flow field the method of mapping the physical plane $z = x + iy$ onto the circle plane $\zeta = \xi + i\eta$ is used. Numerical methods[6,7,8] are available which map an arbitrarily shaped body contour onto a circle by means of the transformation $z = f(\zeta)$. While our work was in progress, Mendenhall, Spangler, and Perkins[9] published a paper on vortex shedding from arbitrarily shaped bodies using a numerical mapping technique for the Theodorsen transformation. V.A. Golovkin and M.A. Golovkin[10] worked with Fredholm integral equations to compute the roll-up of point vortices. In this report exact conformal transformations $f(\zeta)$ are applied to avoid errors due to the approximation of the body contour. Of course, these exact transformations are restricted to certain classes of bodies. For a cylinder with a circular cross-section of radius a and with n evenly distributed fins of length $b-a$, Miles[11] has given $f(\zeta)$ in the implicit form (see Figure 1)

$$z^{(n/2)} + (a^2/z)^{(n/2)} = \zeta^{(n/2)} + (c^2/\zeta)^{(n/2)} \tag{1}$$

$$2c^{(n/2)} = b^{(n/2)} + (a^2/b)^{(n/2)} \tag{2}$$

where c is the radius of the circle in the ζ-plane. Equation (1) can be written in the explicit form

$$z = 2^{-\frac{2}{n}} \{\zeta^{\frac{n}{2}} + (c^2/\zeta)^{\frac{n}{2}} \pm \sqrt{[\zeta^{\frac{n}{2}} + (c^2/\zeta)^{\frac{n}{2}}]^2 - 4a^n}\}^{\frac{2}{n}} \tag{3}$$

In general, this expression is not single-valued and care must be taken in working with it. From Equation (3) it can be shown that $(dz/d\zeta)_{\zeta=\infty} = 1$.

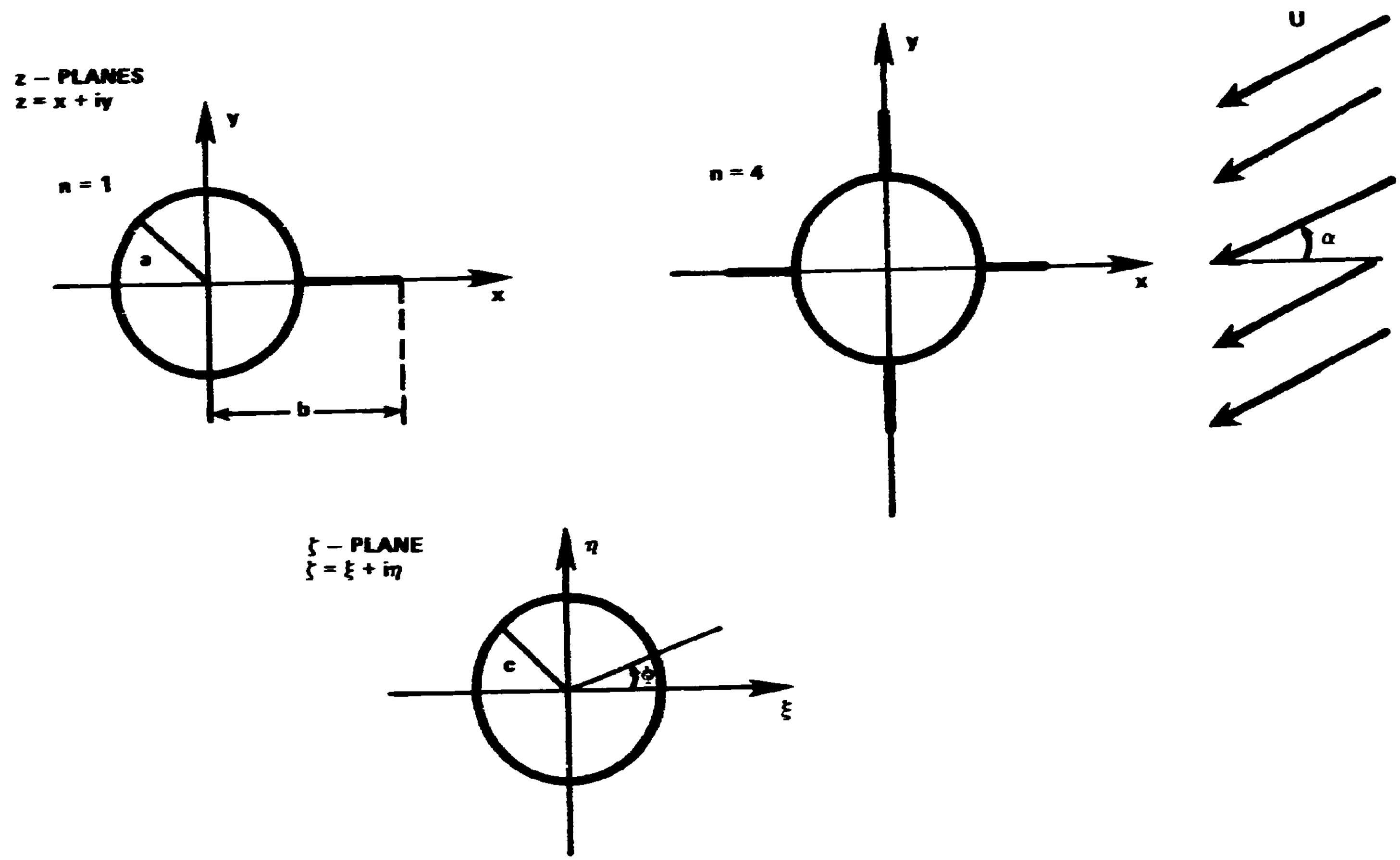

Figure 1 - Conformal Mapping of a Circle with Evenly Distributed Fins in the Radial Direction onto a Circle

For fins protruding in a dihedral configuration at an angle different from 90°, an approximate conformal mapping is given for $n=2$ in implicit form with an auxiliary mapping in the z_2-plane (Figure 2):

$$z + \frac{a^2}{z} = z_2 - \frac{k^2}{z_2} - \left(b + \frac{a^2}{b}\right) \cos \Theta \tag{4}$$

$$z_2 + \frac{r^2}{z_2 - \ell/2} = \zeta + \frac{c^2}{\zeta} + s + \frac{\ell}{2} \tag{5}$$

with

$$k = \frac{1}{2}\left(b - \frac{a^2}{b}\right)\sin \Theta$$

$$\ell = \frac{1}{b}(b - a)^2 \cos \Theta$$

$$r = \sqrt{\frac{1}{2} R\ell}\ , \quad R = \frac{1}{2\ell}\left(\ell^2 + 4k^2\right)$$

$$s = \frac{1}{2}(A_3 + E_3), \quad c = \frac{1}{4}(A_3 - E_3)$$

$$E_2 - \frac{k^2}{E_2} = -2a + \left(b + \frac{a^2}{b}\right)\sin \Theta \text{ for } E_2 < 0$$

$$A_2 - \frac{k^2}{A_2} = 2a + \left(b + \frac{a^2}{b}\right)\sin \Theta \text{ for } A_2 > 0$$

$$A_3 = A_2 + \frac{r^2}{A_2 - \ell/2} - \frac{\ell}{2}$$

$$E_3 = E_2 + \frac{r^2}{E_2 - \ell/2} - \frac{\ell}{2} \tag{6}$$

Here again, $(dz/d\zeta)_{\zeta=\infty} = 1$. The derivation of this conformal transformation is given in Appendix A.

In certain cases, for instance for two fins, the circular cylindrical body can be replaced by an elliptic cylinder:

$$z = z_1 + \frac{p^2 - q^2}{4z_1} \tag{7}$$

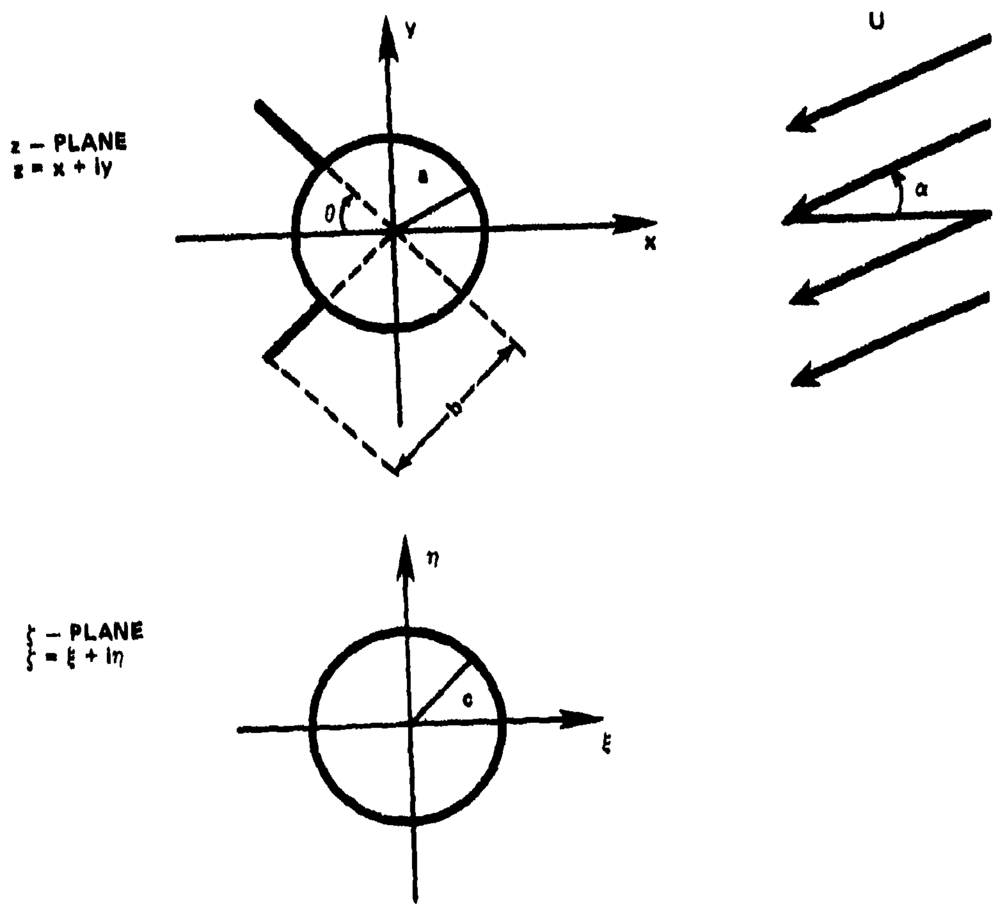

Figure 2 - Conformal Mapping of a Circle with Two Fins in a Dihedral Configuration onto a Circle

$$z_1 + \frac{(p+q)^2}{4z_1} - \ell = \zeta + \frac{c^2}{4\zeta} \tag{8}$$

where

$$\ell = \frac{1}{2}\left[\tau_1 + \frac{(p+q)^2}{4\tau_1} - \tau_2 - \frac{(p+q)^2}{4\tau_2} \right]$$

$$c = \frac{1}{2}\left[\tau_1 + \frac{(p+q)^2}{4\tau_1} + \tau_2 + \frac{(p+q)^2}{4\tau_2} \right]$$

$$\tau_1 = \frac{1}{2}\left(t_1 + \sqrt{t_1^2 - p^2 + q^2}\right)$$

$$\tau_2 = \frac{1}{2}\left(t_2 + \sqrt{t_2^2 - p^2 + q^2}\right) \tag{9}$$

(see Figure 3). Equations (7) through (9) are similar to those given by Bryson.[12] However, Bryson's formulae are not entirely correct, as shown by the case a=b, $t_1 = t_2 = a$, s arbitrary (in Bryson's notation).

3. FLOW FIELD

3.1 COMPLEX POTENTIAL AND COMPLEX VELOCITY

In the problem under consideration the complex potential $w = \Phi + i\psi$, where Φ is the potential function and ψ the stream function, can be written as

$$w = w_p + w_V + w_R \tag{10}$$

where w_p represents the parallel flow around the body, w_V is the contribution due to the presence of m vortices, and w_R is the term which takes account of the rotation of the body. Since the complex potential is by definition the same in the z- and ζ-planes, the contribution due to parallel flow is[13]

$$w_p = U\left(\zeta e^{-i\alpha} + \frac{c^2}{\zeta} e^{i\alpha}\right) \tag{11}$$

with U the constant velocity of the parallel flow and α the angle of attack measured counterclockwise from the positive real axis. The term w_V representing the m vortices is given by

$$w_V = i \sum_{k=1}^{m} \kappa_k \left[\log(\zeta - \zeta_k) - \log\left(\zeta - \frac{c^2}{\bar{\zeta}_k}\right)\right] \tag{12}$$

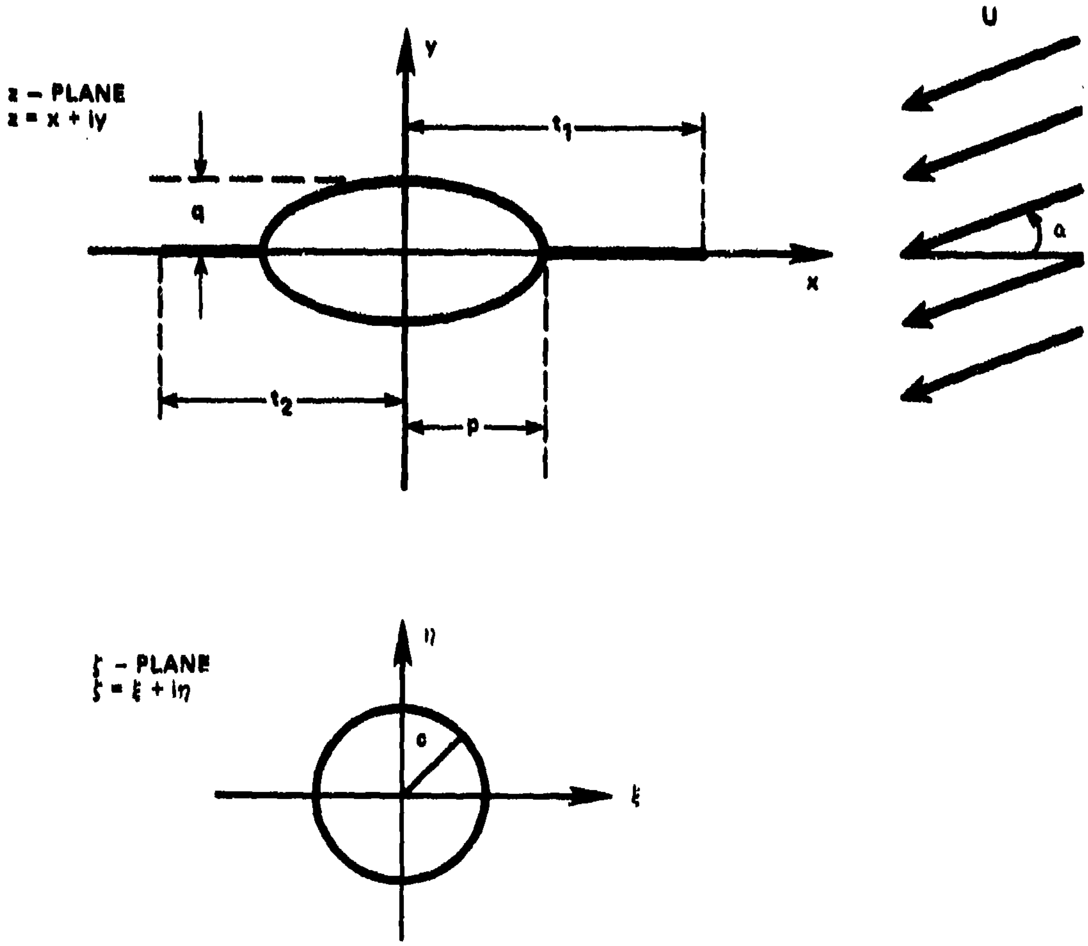

Figure 3 - Conformal Mapping of an Ellipse with Two Fins onto a Circle

where κ_k denotes the strength of the k^{th} vortex and ζ_k its position. $\bar{\zeta}_k$ is the complex conjugate of ζ_k.

The contribution w_R can be obtained with a method described by Milne-Thomson.[13] For a body rotating with angular velocity $\omega(t)$, the stream function at a point σ of the circle is given by

$$2i\psi = i\omega z\bar{z} = i\omega\, f(\sigma)\, \bar{f}(\frac{c^2}{\sigma}) = i\omega\, B(\sigma) \tag{13}$$

where $B(\sigma)$ is called the boundary function. If $B(\sigma)$ is written in the form of a Laurent series in σ, then $B(\sigma) = B_1(\sigma) + B_2(\sigma)$ where B_1 contains the negative powers of σ and B_2 the non-negative powers. With the aid of Cauchy's residue theorem[13] it follows that

$$w_R(\zeta) = i\omega\, B_1(\zeta) \tag{14}$$

Bryson[12] has discussed $B_1(\zeta)$ for the case covered by Equation (3). The general situation $a \neq 0$ requires the evaluation of a double sum which converges slowly near the body and more rapidly farther away (see Appendix B). For $a = 0$ this double sum can be reduced according to Bryson[12] to

$$B_1(\zeta) = \sum_{\ell=1}^{\infty} \frac{(-1)^{\ell+1}}{\pi\zeta^n}\, \Gamma(1+\frac{4}{n})\, c^{n\ell+2}\, \frac{\Gamma(\ell-\frac{2}{n})}{\Gamma(\ell+\frac{2}{n}+1)}\, \sin\frac{2\pi}{n}, \quad (a=0) \tag{15}$$

where Γ is the gamma function. This expression is undetermined for $n = 1$ and 2. However, one easily obtains from Equation (3):

$$B_1 = 4\,\frac{c^3}{\zeta} + \frac{c^4}{\zeta^2} \quad \text{for } n=1,\ a=0 \tag{16}$$

$$B_1 = \frac{c^4}{\zeta^2} \quad \text{for } n=2,\ a=0 \tag{17}$$

The angle of attack α is related to the angular velocity ω by

$$\alpha = \alpha_0 + \int_0^t \omega\, d\tilde{t} \tag{18}$$

The complex conjugate velocity of the flow is given, except for the point vortices themselves, by:

$$\frac{d\bar{z}}{dt} = u - iv = -\frac{dw}{dz} = -\frac{dw}{d\zeta}\frac{d\zeta}{dz} \tag{19}$$

where

$$\frac{dw}{d\zeta} = U(e^{-i\alpha} - \frac{c^2}{\zeta^2} e^{i\alpha}) + i \sum_{k=1}^{m} \kappa_k (\frac{1}{\zeta-\zeta_k} - \frac{1}{\zeta - \frac{c^2}{\bar{\zeta}_k}}) + i\omega \frac{dB_1}{d\zeta} \tag{20}$$

$$\frac{d\zeta}{dz} = \frac{z^{\frac{n}{2}-1} - a^n z^{-\frac{n}{2}-1}}{\zeta^{\frac{n}{2}-1} - c^n \zeta^{-\frac{n}{2}-1}} \tag{21}$$

The velocity of the k^{th} vortex is, according to Routh's theorem (Milne-Thomson[13]),

$$\frac{d\bar{z}_k}{dt} = \frac{d\bar{\zeta}_k}{dt} \cdot \frac{d\zeta_k}{dz_k} - \frac{i}{2} \kappa_k \frac{d}{d\zeta_k} (\frac{d\zeta_k}{dz_k}) \tag{22}$$

with

$$\frac{d\bar{\zeta}_k}{dt} = -(\frac{dw}{d\zeta})_{\zeta_k} + i \frac{\kappa_k}{\zeta-\zeta_k}$$

When the reference frame is to be fixed to the body, the solid-body rotation $w = -\frac{i}{2}\omega\bar{\zeta}$ must be added to the terms in Equation (10). The corresponding velocity is

$$\frac{d\zeta}{dt} = i\,\omega\,\bar{\zeta} \tag{23}$$

3.2 DIMENSIONLESS FORM OF THE COMPLEX VELOCITY

The complex velocity of the flow field, including that of the vortices, Equations (19) and (22), is made dimensionless by U. For the coordinates and other quantities with the dimension of length, the parameter 2b is chosen as the characteristic length. In particular, the time t is made dimensionless by U/2b and the vortex strength κ by 1/2b U. The same notation is used for the nondimensional quantities in the results (Section 6).

4. VORTEX GENERATION AND SHEDDING

4.1 FEEDING MECHANISM

The process of vortex generation requires the existence of a boundary layer and its separation from the body. After separation the boundary layer becomes a free shear layer in which vorticity is concentrated in a thin layer for high Reynolds numbers. Such a layer rolls up in time by forming a vortex. In potential flow, which does not allow the creation and elimination of vorticity, the roll-up is modeled by a discontinuity line. Self-similarity of the discontinuity spiral with advancing time is assumed for the initial period when the finiteness of the plate is not yet felt. This idea goes back to Prandtl.[14] More recently, detailed studies were made by Wedemeyer,[15] Blendermann,[16] and Pullin.[17] The discontinuity spiral close to the center has the form $r \approx \phi^{-2/3}$ and is, therefore, a hyperbolic type of spiral with infinitely many turns.

Numerically, the discontinuity line itself is often approximated by a row of point vortices (discrete-vortex model). Earlier difficulties with such a model have been largely overcome by a rediscretization procedure developed by Fink and Soh.[1] This method is used in the present work.

At the sharp edge of a body flow always separates when it meets the body under a nonzero angle. The discontinuity line originates at the sharp edge. It grows in time with new line elements forming at the edge. In a discrete-vortex model new point vortices are introduced after the time interval Δt. The feeding mechanism works in the following way:

(a) At time $t+\Delta t$ vortices are convected away from the edge. Their new positions are computed with the aid of Equation (22).

(b) Each discontinuity line is rediscretized in the physical plane so that every vortex on it lies at the center of the segment represented by the vortex. If s_k is the distance of vortex k along the line from the first vortex on the line, then the total length S of the line is s_M, where M is the number of vortices on the line. The segment length after rediscretization is given by $\Delta\hat{s} = S/(M-1)$ and so the new positions of the vortices can be calculated from

$$\hat{s}_k = (k-1)\Delta\hat{s} \tag{24}$$

where $\hat{s}_k$ is the distance after rediscretization of vortex k from the first vortex on the line. The positions of the first and last vortices are unchanged by the rediscretization procedure.

(c) The strengths of the vortices are recalculated according to Shouff[18] to account for the changed positions of the vortices. First, the strength density γ_k near each vortex before rediscretization is computed as

$$\gamma_k = \begin{cases} \kappa_1/(s_2 - s_1) & \text{if } k=1 \\ 2\kappa_k/(s_{k+1} - s_{k-1}) & \text{if } 1<k<M \\ \kappa_M/(s_M - s_{M-1}) & \text{if } k=M \end{cases} \tag{25}$$

For the redistributed vortices, the strength density is approximated by

$$\hat{\gamma}_k = \gamma_{\ell-1} + (\gamma_\ell - \gamma_{\ell-1}) \frac{\hat{s}_k - s_{\ell-1}}{s_\ell - s_{\ell-1}} \tag{26}$$

where ℓ has been determined so that $s_{\ell-1} \leq \hat{s}_k < s_\ell$. Thus, the strengths of the redistributed vortices are $\hat{\gamma}_k \Delta\hat{s}$ to a first approximation. But since the procedure outlined so far does not necessarily conserve the total vortex strength in each discontinuity line, the deficit or excess strength is removed by adding an equal amount of strength to each vortex. Hence, the new strengths are given by

$$\hat{\kappa}_k = \hat{\gamma}_k \Delta\hat{s} + \frac{1}{M} \left(\sum_{\ell=1}^{M} \kappa_\ell - \sum_{\ell=1}^{M} \hat{\gamma}_\ell \Delta\hat{s} \right) \tag{27}$$

(d) In each discontinuity line a new vortex is introduced between the edge and the first vortex at a point 1/3 of the distance from the edge in the physical plane. The ζ-plane positions of all the vortices are calculated. Then the strengths of the nascent vortices are determined by satisfying the Kutta-Joukowsky condition

$$\left(\frac{dw}{d\zeta}\right)_{\zeta=\zeta_i} = 0 \tag{28}$$

at each fin tip ζ_i in the ζ-plane. For n fins n linear equations of Equation (28) type must be solved.

Accuracy is checked by computing the shape and position of the vortex spiral and the increase of the total vortex strength at the i^{th} fin with time for various Δt:

$$K_i(t) = \sum_{k=1}^{M} \kappa_{ik} \tag{29}$$

Figure 4a shows that with decreasing Δt the number of the inner loops increases, but this does not seriously affect the shape and location of the spiral or its strength (see Section 6 and Figures 4a, b, c).

4.2 INITIAL CONDITION

Starting a vortex sheet at $t=0$ in a potential flow of constant velocity U corresponds to the abrupt start of the body from rest to the velocity $-U$. The initial sheet for $t = \Delta t$ can be taken from the self-similar solution for a vortex spiral behind the edge of a semi-infinite plate. A trial-and-error approach, however, shows that the development of the spiral row of point vortices is quite insensitive to the placement of the first vortex with respect to the subsequent roll-up. The strength of the first vortex again is determined by the Kutta-Joukowsky condition (28). The location of the first vortex, which is arbitrary, can be described by the distance Δs away from the tip and the angle β between the extension of the fin and the line drawn from the tip to the vortex. Although variation in Δs (from $\Delta s = 0.025$ to 0.03) was not noticeable in the results, small but still insignificant differences occurred when β was varied (Figure 5).

4.3 CUT-OFF PROCEDURES

The infinite turns in the vortex spiral cannot be represented by a row of point vortices, and these turns are physically unrealistic anyway (Section 4.4). Somewhere the spiral has to be cut off. Investigations by Wedemeyer[15] and Pullin[17] have revealed that the almost circular windings, which represent the core of the vortex, can be replaced by a single vortex. Even this single vortex appears not to be necessary (Fink and Soh[1]). The overall solution is quite insensitive to arbitrary cut-off.

Another cut-off procedure is necessary when the rolled-up spiral separates from the body and becomes a detached vortex which swims away in the wake. Although the development of a vortex row without the use of the rediscretization technique somehow takes care of this separation by itself (see Figure 7b, page 21), the line of redistributed vortices has to be severed by a proper criterion. Shoaff[18] uses the condition $d\kappa/dt = \min$ after a certain developing time of the vortex row. This criterion has been applied here with varying success (see Section 6). The detached line is, by the way, also rediscretized. Shoaff's technique of replacing the detached line after two body lengths by a single vortex has also been adopted.

Figure 4 - Accuracy Tests with Flows Past a Flat Plate at $\alpha = 90°$

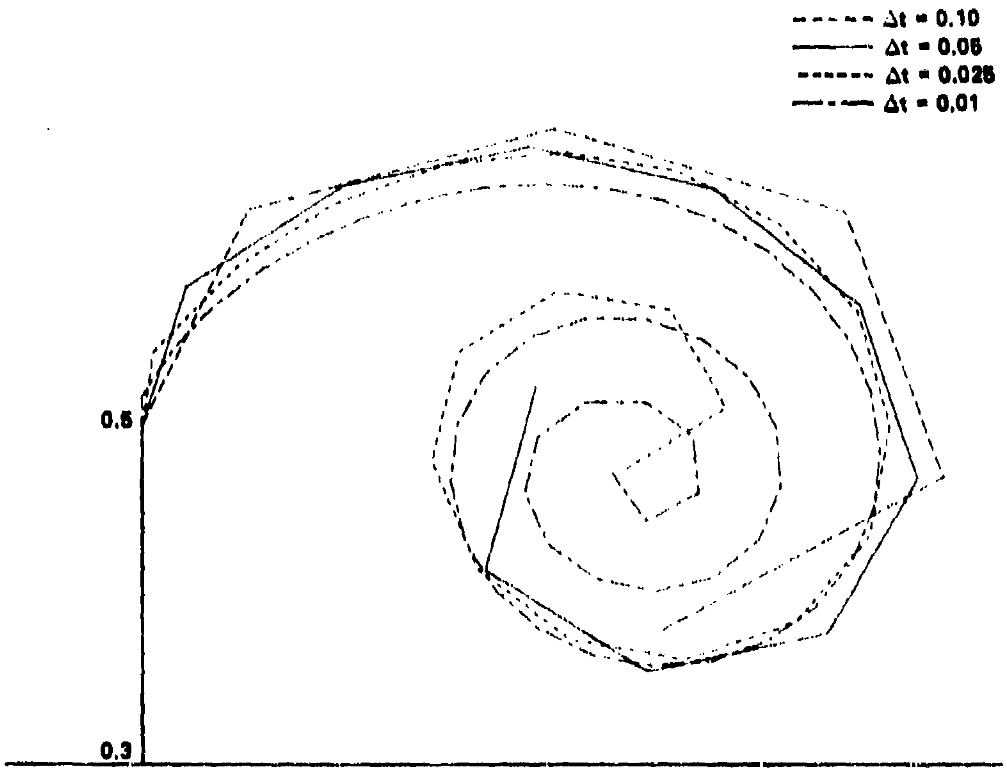

Figure 4a - Discontinuity Lines at $t = 0.5$ for Various Δt

Figure 4 (Continued)

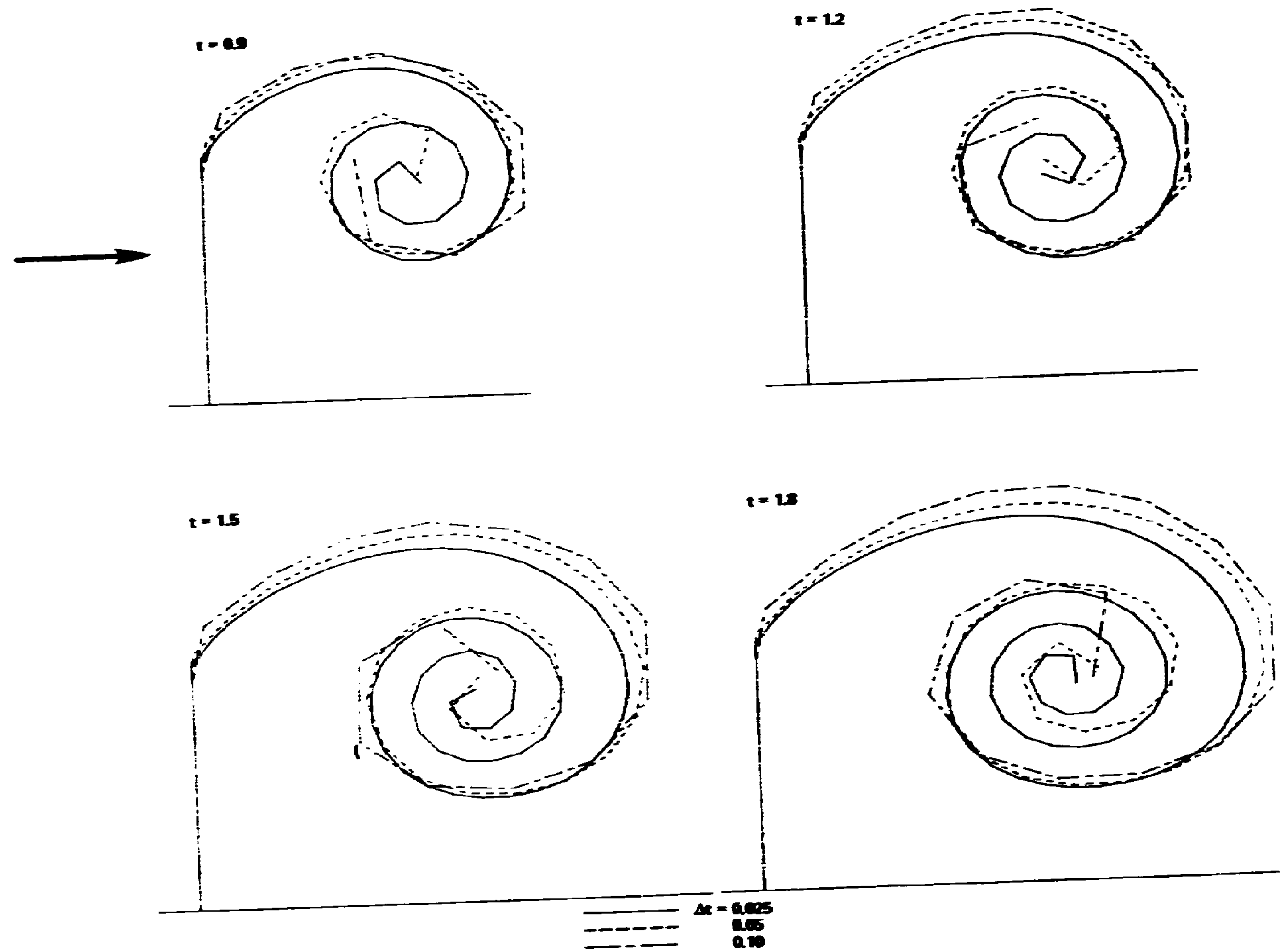

Figure 4b - Sequence of Discontinuity Lines at Selected Times for Various Δt

Figure 4 (Continued)

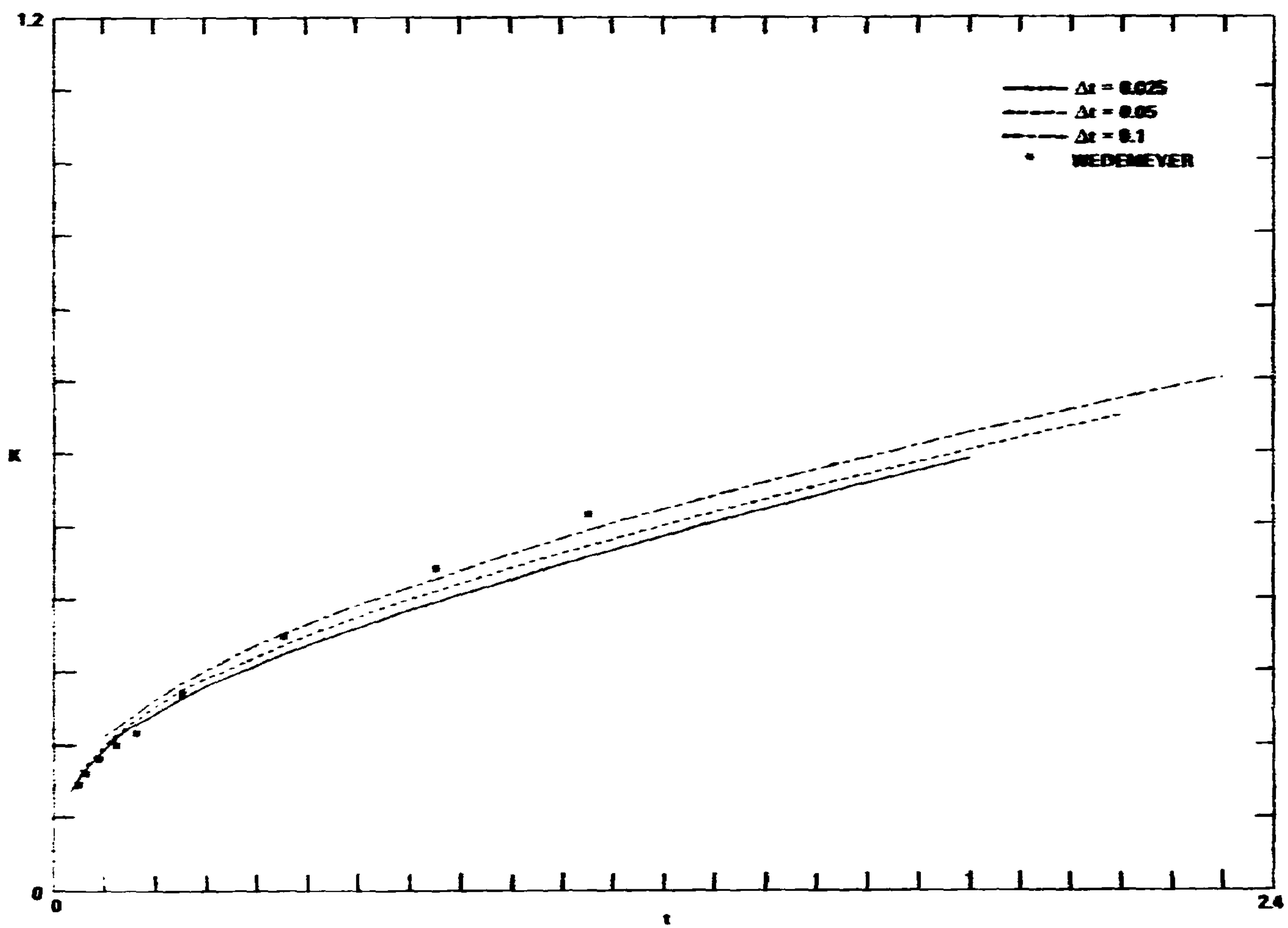

Figure 4c - Total Strength of One Edge Vortex for Various Δt. Comparison with Wedemeyer's Result.

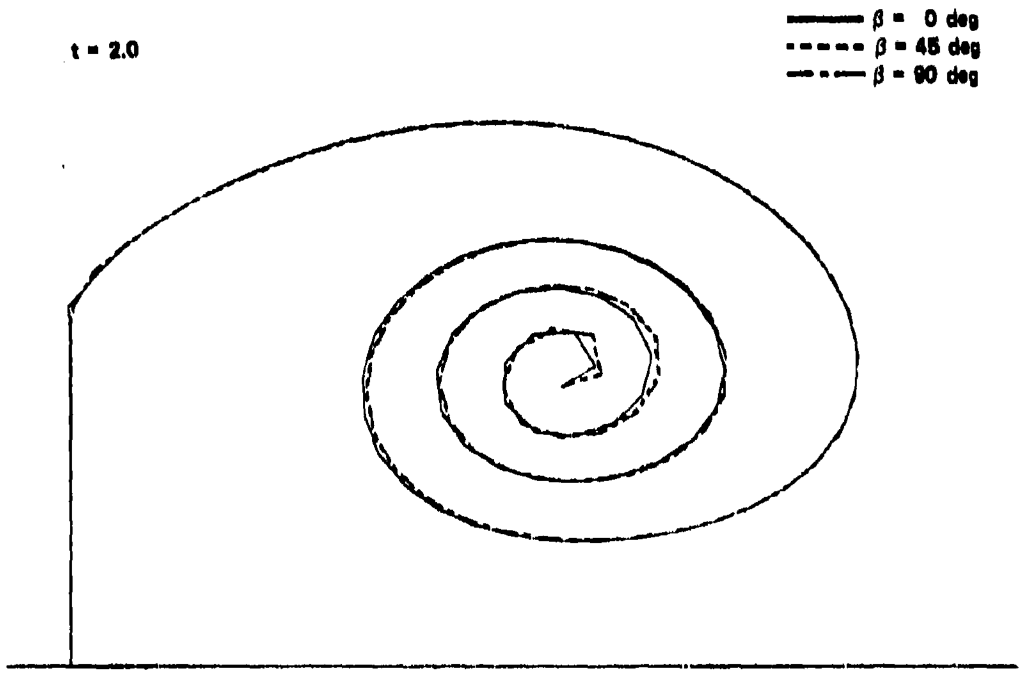

Figure 5 - Accuracy Tests with Flows Past a Flat Plate at $\alpha = 90°$ for Various Initial Conditions. Discontinuity Lines at $t = 2$ with $\Delta t = 0.025$ for Three Different β's.

4.4 VISCOUS EFFECTS

The neglect of viscosity may restrict the usefulness of the model. There are three major flow regions in which viscosity cannot be ignored, and the influence of such neglect on the overall flow characteristics must be questioned.

Infinitely many turns of the vortex spiral are obviously not realistic, since during the creation of the vortex the core is in a state of solid-body rotation. Moore and Saffman[19] have discussed the structure of the vortex spiral and have given estimates of the viscous core which is present from $t=0$ on. After separation from the body the vortex decays through dissipation, and this effect is not simulated in the point-vortex model either.

Vortices or blobs of vorticity of opposite sign, which approach each other, are eliminated or coalesce in a viscous fluid. Also, when vortices approach a solid surface, they are weakened or destroyed by the opposite vorticity produced at the wall. None of these effects are simulated in the inviscid-flow model.

4.5 OTHER SEPARATION POINTS

So far, flow separation has been considered only at the tips of the fins. However, other separation points at the body surface may occur as, for instance, in the case of the circular cylinder with one fin. Here, a separation point must exist on the side of the body opposite the single fin. Separated regions may also appear between fins when $n > 1$.

The occurrence of separation points can be predicted with the aid of boundary-layer theory. Such a prediction method, together with a technique to provide for a vortex sheet at the separation point, will be included in the computer code at a later time.

5. FLOW CHART

The sequence of computations is indicated in the following flow chart. The calculation of force coefficients is included.

6. SOME RESULTS

A computer program based on the equations of Sections 2 through 5 has been developed for circular cylinders under the restriction $n \leq 4$. However, most cases of practical interest are covered under this restriction.

FLOW CHART

$t = t + \Delta t$

↓

CONVECT VORTICES

↓

REDISCRETIZE VORTEX SHEETS

↓

INTRODUCE NASCENT VORTICES

↓

LOCATE VORTEX POSITIONS
IN THE COMPUTATIONAL PLANE

↓

DETERMINE NASCENT VORTEX STRENGTHS

↓

COMPUTE VELOCITIES OF THE VORTICES
IN COMPUTATIONAL AND PHYSICAL PLANES

↓

CALCULATE FORCE AND MOMENT COEFFICIENTS

↓

OUTPUT

Two samples have been selected for comparing results of the present computer program with those from the literature. A third example gives new results. More complicated cases of practical interest will be published later.

6.1 VORTEX SHEDDING FROM A FLAT PLATE AT $\alpha = 90°$

This case is of particular interest since its results can be compared with results of Fink and Soh,[1] which are based on a similar point-vortex method, and with analytical results of Wedemeyer[15] for a discontinuity line, at least for the initial phase of the roll-up. The results are presented in Figures 4c and 6.

In Figure 6 the roll-up of the discontinuity line is shown at times t - 0.25, 0.5, 0.75, 1.0, and 1.5 with $\Delta t = 0.02$. Up to $t = 0.75$ the curves are compared with Wedemeyer's self-similar solution,[15] which is valid for a semi-infinite plate. From $t = 0.75$ on, deviations occur because of the influence of the finiteness of the plate width. (According to Wedemeyer[15] differences between infinitely wide and finite-width plates become noticeable from $t = 0.6$ on.) For $t = 1.0$ and 1.5 the results are compared with those of Fink and Soh.[1] The agreement is quite good. In all cases the limiting curve for $t = \infty$ by Helmholtz is shown, along which the discontinuity spiral rolls up until it becomes unstable. It may be mentioned that in this early phase the flow is symmetric, and no attempt has been made to induce alternating vortex shedding through an initial asymmetric disturbance.

In Figure 4c the increase in total vortex strength K with time for one half of the plate is compared with the corresponding result by Fink and Soh.[1] Their data are slightly larger and agree with those of Wedemeyer for a plate of finite width.

6.2 VORTEX SHEDDING FROM A FLAT PLATE AT $\alpha = 45°$

Results for this case can also be compared with those in the literature. In Figure 7 the roll-up of the discontinuity line is shown for $t = 0.5$, 1.0, and 2.0 with $\Delta t = 0.05$ and is compared with the curves by Belotserkovskii and Nisht,[20] who did not use a rediscretization procedure. The advantage of rediscretization is particularly demonstrated for the roll-up behind the leading edge. In Figure 8 the same situation is presented at the slightly different times $t = 0.39$, 1.12, and 1.87 and the results are compared with the corresponding solutions of the Navier-Stokes equations for $Re = 2bU/\nu = 200$. The flat plate is here approximated by a thin elliptic cylinder of infinite length with a width-to-thickness ratio of 10 to 1. A discussion of the differences has already been published.[21]

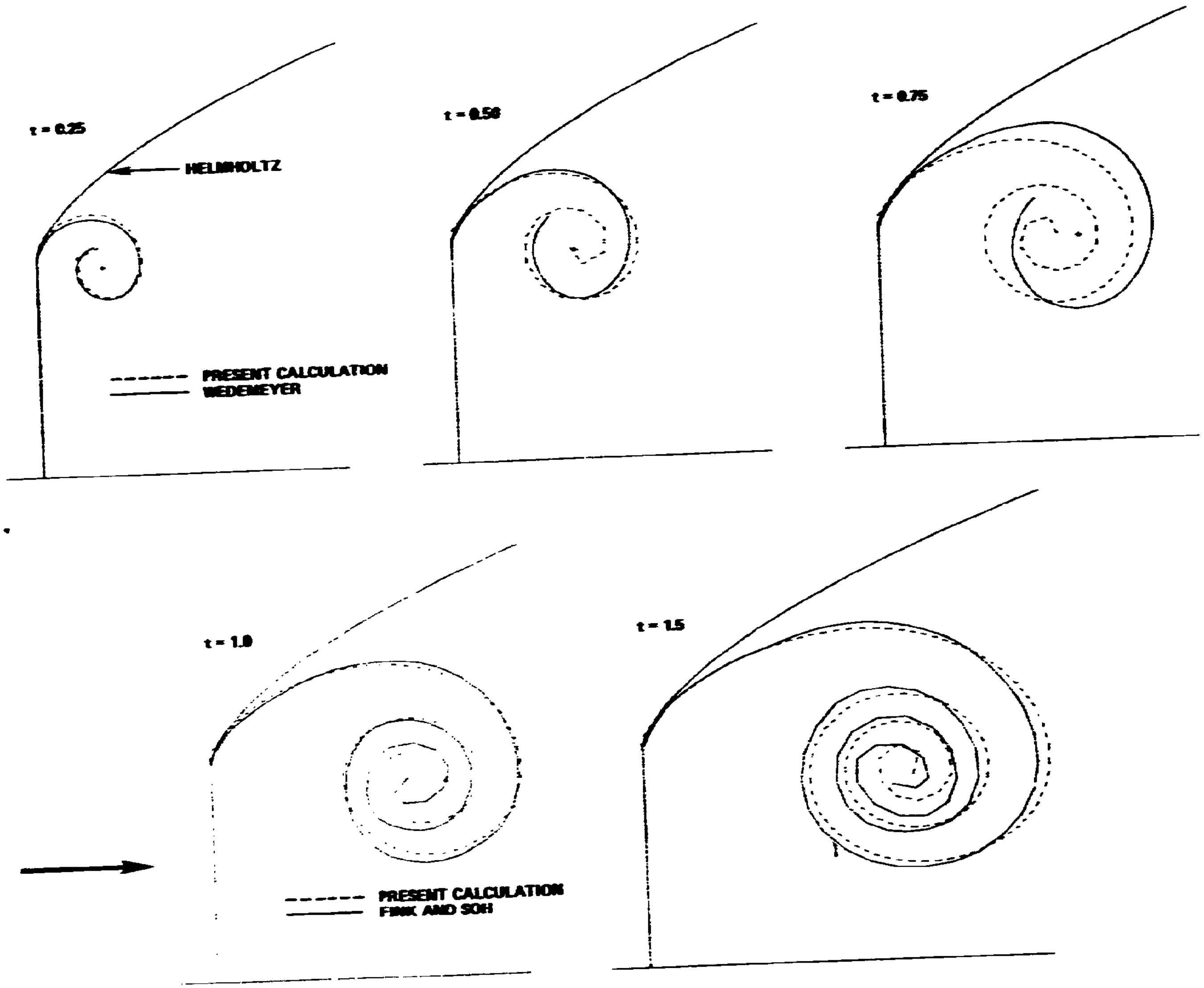

Figure 6 – Development of Discontinuity Lines Behind a Flat Plate for $\alpha = 90°$. Comparison with Wedemeyer's[15] and Fink and Soh's[1] Results.

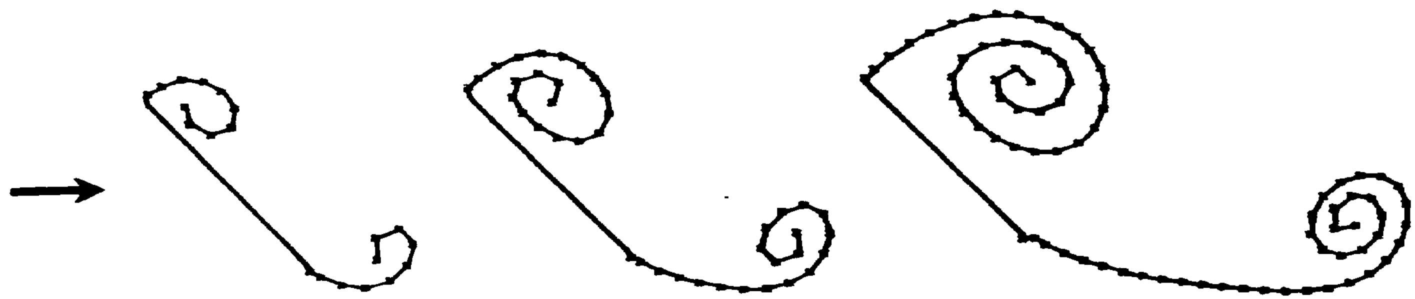

Figure 7a - Present Results

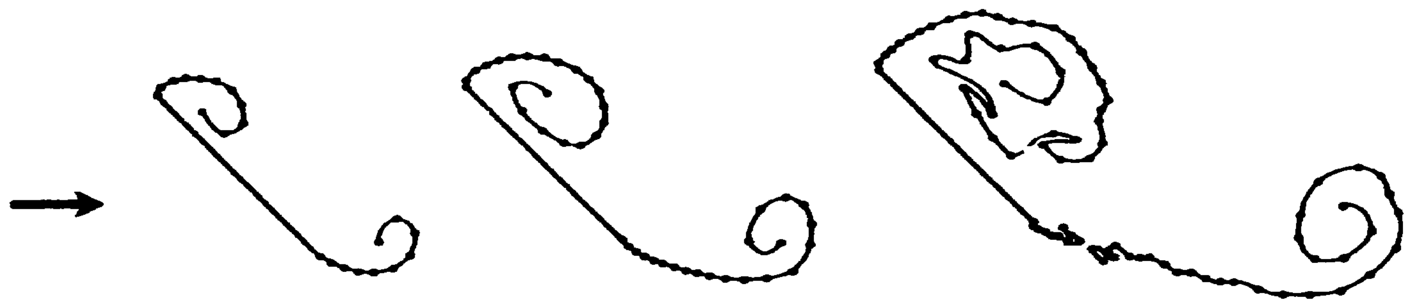

t = 0.5 t = 1.0 t = 2.0

Figure 7b - Comparison with Belotserkovskii and Nisht's[28] Results

Figure 7 - Development of Discontinuity Lines Behind a Flat Plate at $\alpha = 45°$

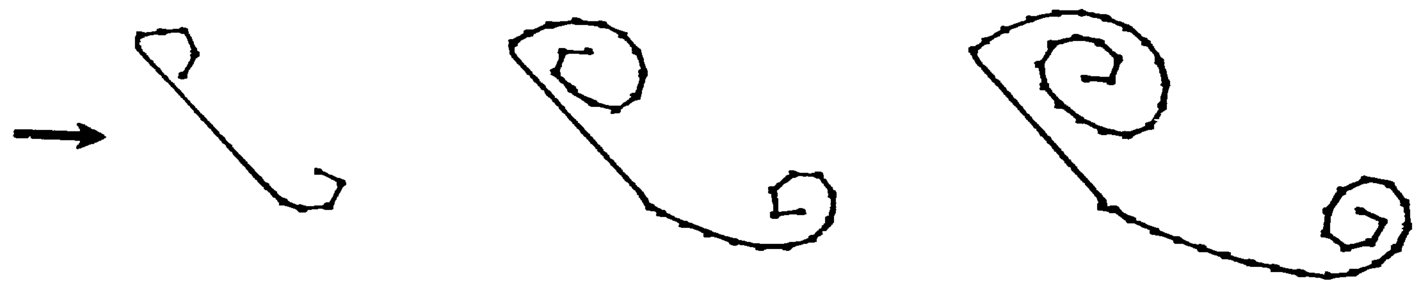

Figure 8a - Present Results

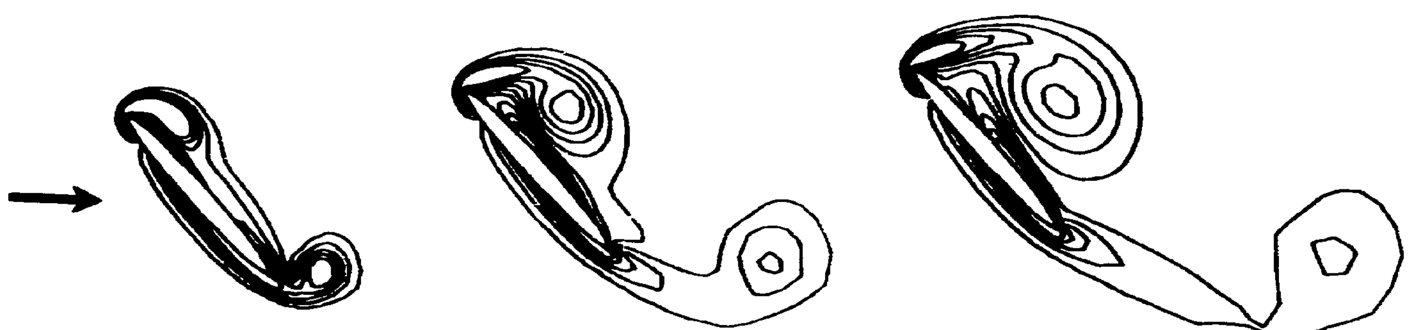

Figure 8b - Comparison with Solutions of the Navier-Stokes Equations for Re = 200, Thin Elliptic Cylinder[21]

Figure 8 - Development of Discontinuity Lines Behind a Flat Plate at $\alpha = 45°$

In Figure 9a the total strength K_1 of the leading-edge vortex is compared with that of the trailing-edge vortex K_2. The absolute amount of the latter is slightly smaller so that the sum of the two is not zero (Figure 9b). This violates the conservation law of vorticity. In reality, however, boundary layers contribute to the generation of vorticity which would account for the difference. In an inviscid-flow model a bound vortex can be introduced at the center of the circle to balance the difference. This technique was studied with the present computer program. Since the results were not significantly different, the incorporation of such a bound vortex was abandoned.

Difficulties have been encountered with the cut-off procedure. The trailing-edge vortex could be separated with Shoaff's criterion (Section 4.3) and could simulate vortex shedding satisfactorily. However, the leading-edge vortex did not move away fast enough after cut-off and interfered with the development of the new vortex sheet. The problem has not yet been solved, but it may be a consequence of the rediscretization procedure.

6.3 VORTEX SHEDDING FROM A CIRCULAR CYLINDER WITH TWO FINS AT $\alpha = 45°$

In the final example the vortex shedding from a circular cylinder with two fins at $\alpha = 45°$ was compared with that from a flat plate at $\alpha = 45°$. Figure 10 displays the development of the discontinuity lines for both cases. Up to $t = 0.6$ the leading-edge vortices do not show any visible differences, but the trailing-edge vortex for the flat plate is slightly stronger. Beyond $t = 0.6$ the leading-edge vortex is deformed by the presence of the cylinder. The corresponding data for the total strengths K_1 and K_2 in Figure 9 confirm that K_2 is slightly smaller than K_2 for the flat plate.

The two-dimensional time development of the discontinuity line in Figure 10 can also be interpreted as a spacial growth in a three-dimensional flow within the frame-work of a strip theory. Then, t is replaced by the coordinate Z perpendicular to the x,y-plane with the aid of the constant velocity W in the Z-direction: $t = Z/W$. A computer-generated perspective view is presented in Figure 11.

Figure 9 – Total Strengths of the Vortices at the Leading and Trailing Edges for Flows Past a Flat Plate and Past a Circular Cylinder with Two Fins at $\alpha = 45°$

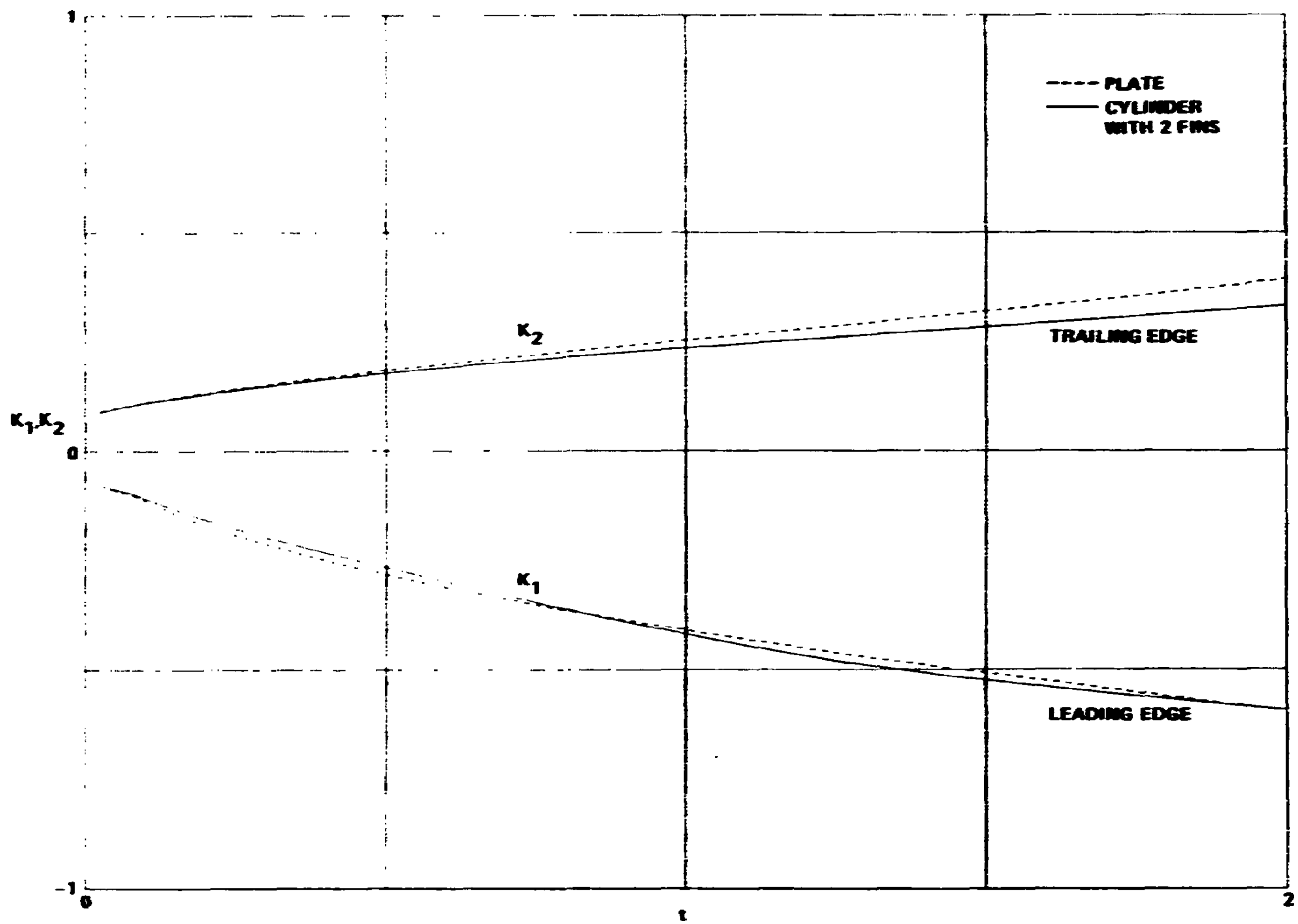

Figure 9a – K_1, K_2 Plotted versus t with $\Delta t = 0.025$

Figure 9 (Continued)

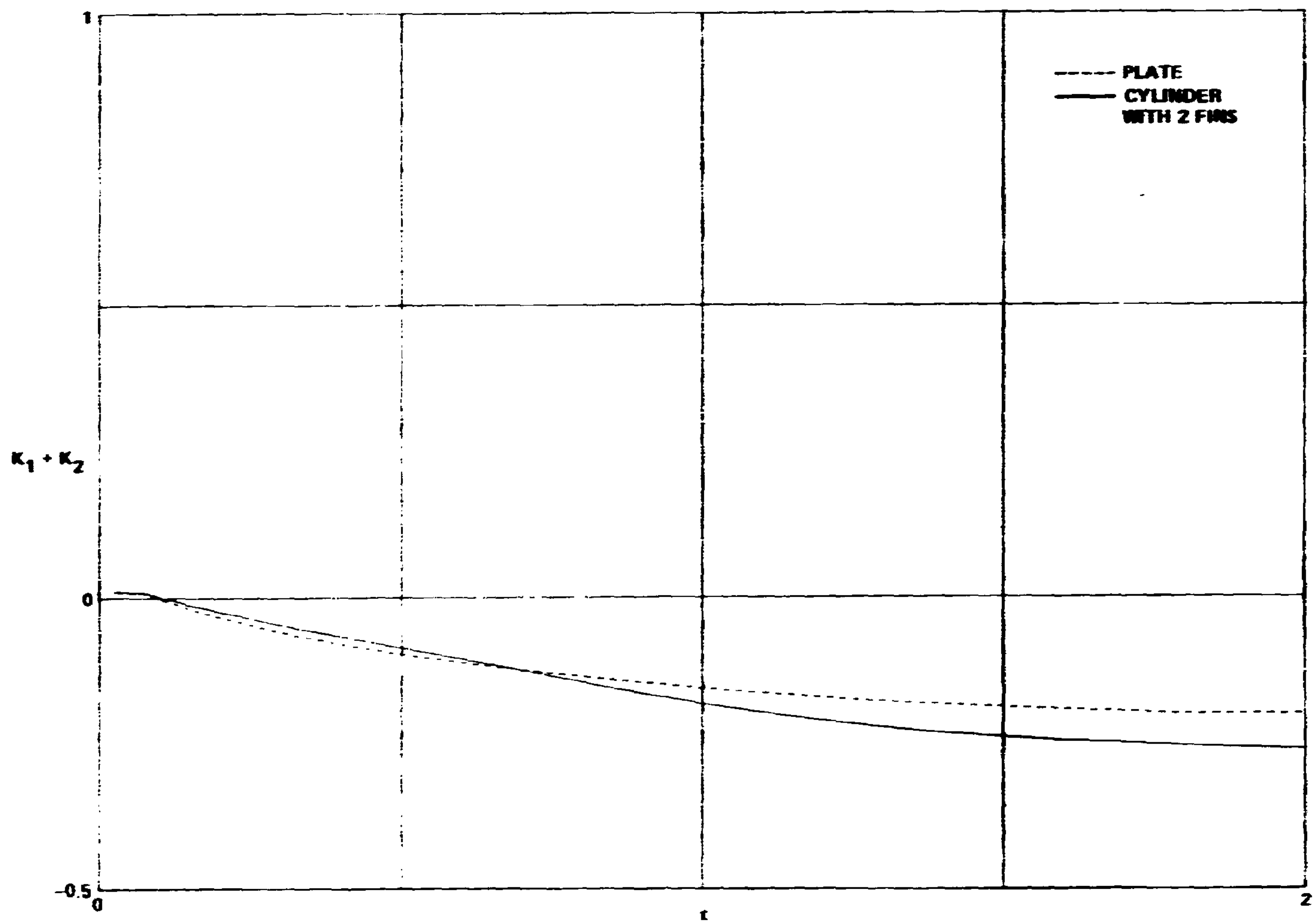

Figure 9c - Same Situation as in Figure 9a. Difference of the Total Strengths of the Vortices at the Leading and Trailing Edges.

Figure 10 - Development of Discontinuity Lines Behind a Circular Cylinder with Two Fins at $\alpha = 45°$ ($n = 2$, $a:b = 2:5$), $\Delta t = 0.02$. Comparison with Flow Past a Flat Plate.

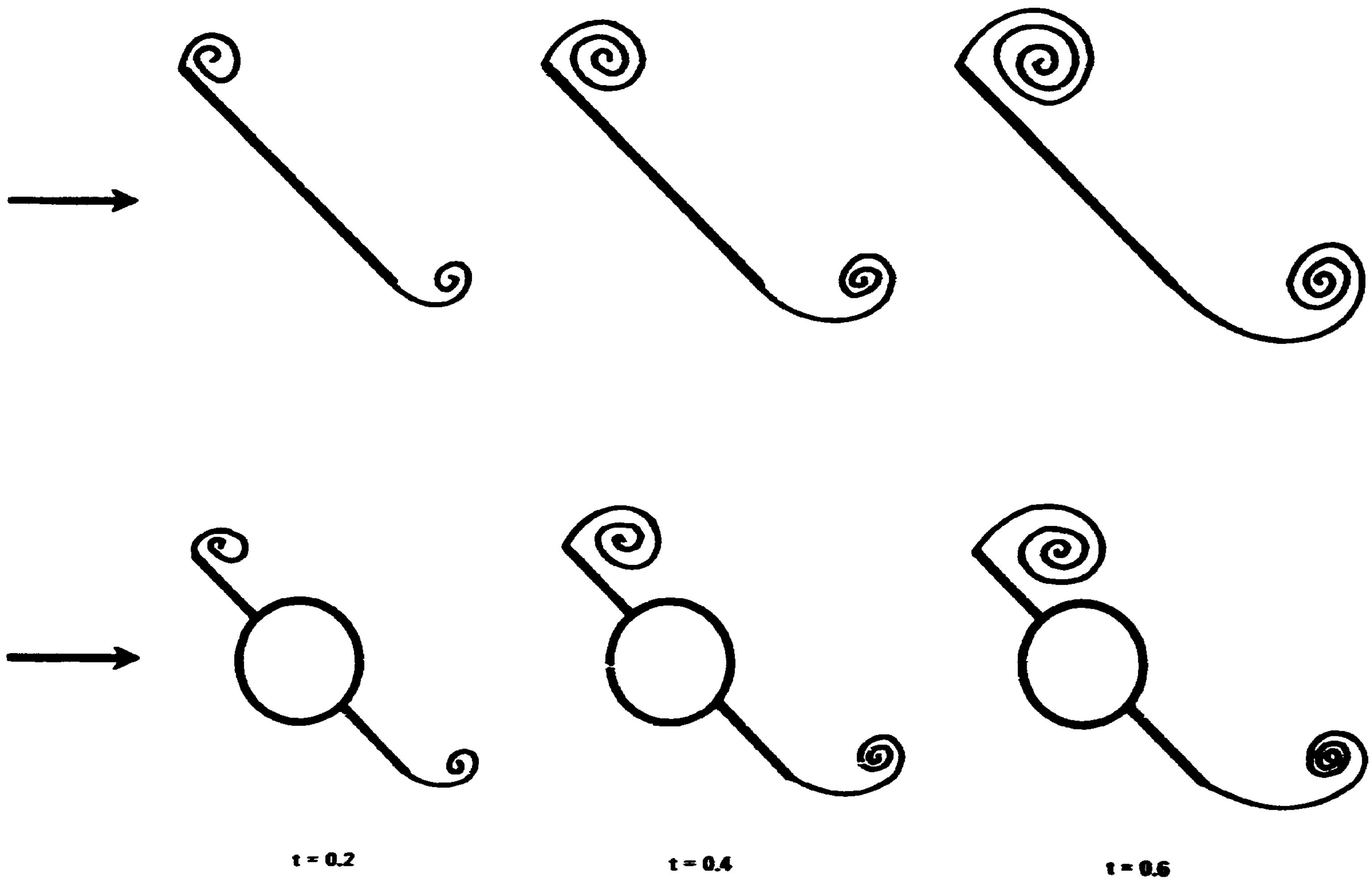

Figure 10 (Continued)

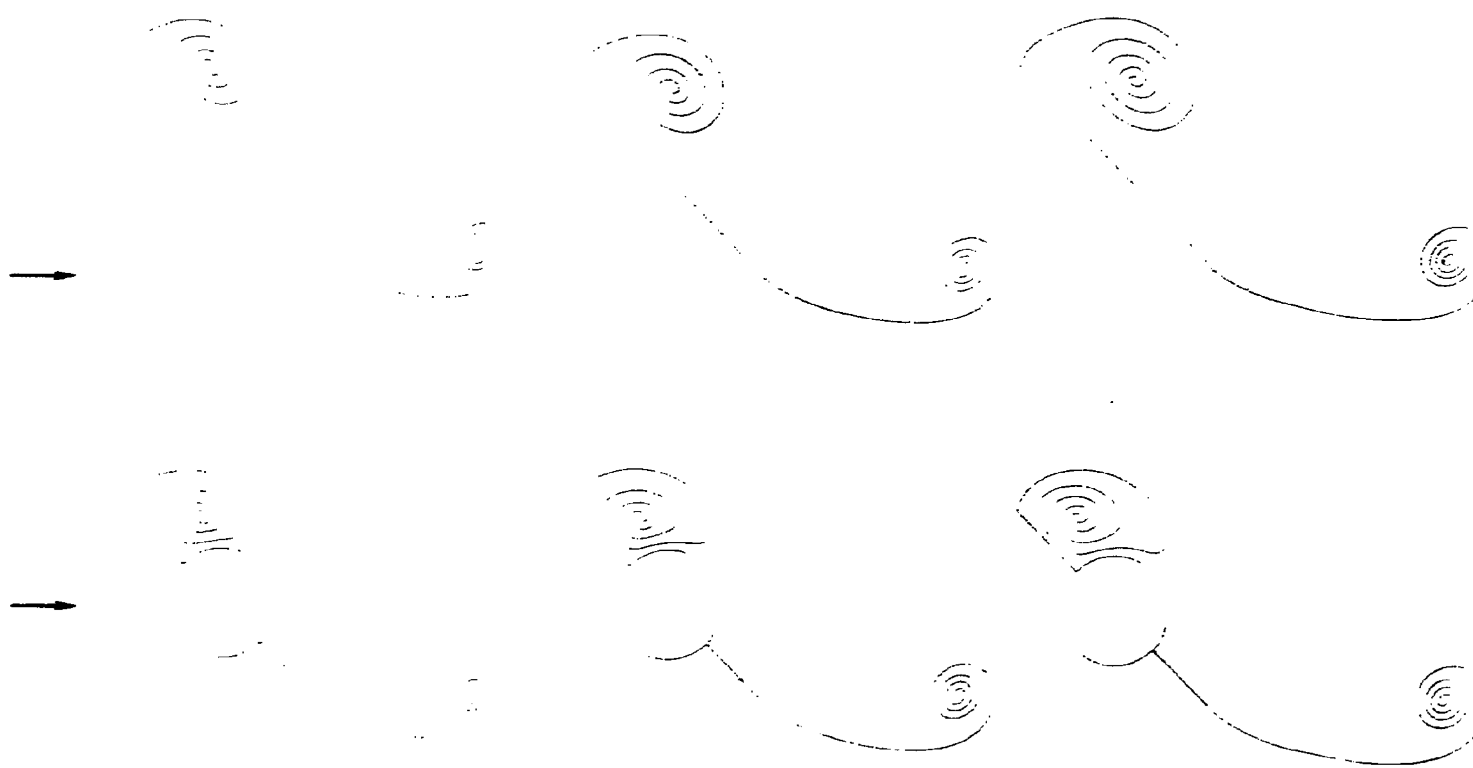

t = 0.8 t = 1.0 t = 1.2

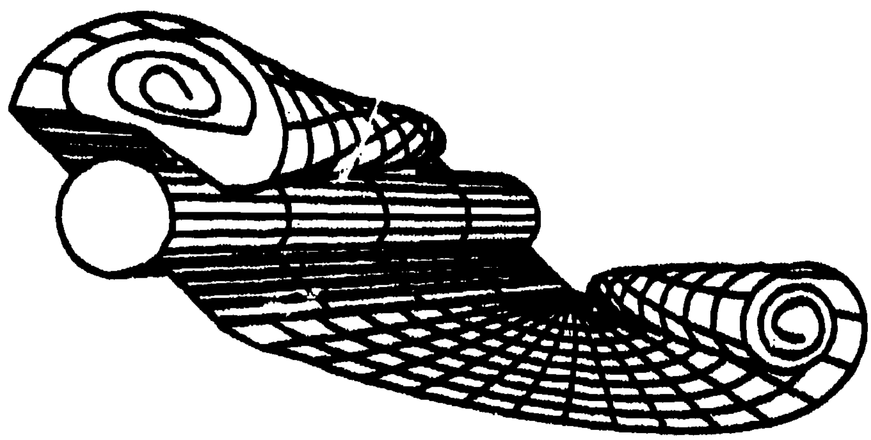

Figure 11 - Projection of the Situation in Figure 10
with the Aid of a Strip Technique

7. CONCLUSIONS AND SUMMARY

a. A computer program has been developed to simulate, by means of a discrete-vortex model, vortex shedding from a circular cylinder with up to four evenly distributed fins.

b. A new approximate conformal transformation for a circular cylinder with two dihedral fins (Figure 2) has been derived, and a conformal transformation for an elliptic cylinder with two fins has been improved (Section 2).

c. A numerical method has been devised for computing the coefficients of the Laurent series, which are necessary to find the potential function for the rotational motion of the body (Section 3.1 and Appendix B).

d. The feeding mechanism, that is, the introduction of the new point vortex near the tip at each time step, is the crucial process in the whole model. Although the shape and the location of the spiral discontinuity lines are quite insensitive to various approximation schemes, the strengths of the discrete vortex rows are somewhat weaker than those reported by Wedemeyer[15] and Fink and Soh.[1]

e. Although results for the force coefficients are not reported here, preliminary studies indicate that they are very sensitive to the kind of feeding mechanism used. This is also reflected in the different results of Belotserkovskii and Nisht[20] and Sarpkaya[22] for the vortex shedding from an inclined plate.

f. The CP time in seconds on the TI-ASC is equal to $0.003\, m^2$ for bodies with two fins.

8. PROPOSED EXTENSIONS AND REFINEMENTS TO THE PROGRAM

The usefulness of the computer program described can be enhanced by incorporating the following extensions and refinements:

a. Include the roll-up of discontinuity lines shed from the cylinder (other than the tips of the fins). This requires building in a boundary-layer code for determining the point of separation and the amount of vorticity shed at that point.

b. Improve the feeding mechanism to obtain reliable force and moment coefficients.

c. Include the computation of force and moment coefficients.

d. Investigate viscous effects and make appropriate corrections.

e. Consider other conformal transformations of practical interest.

ACKNOWLEDGMENTS

The authors owe thanks to Drs. R.L. Shoaff and H.J. Haussling for many fruitful discussions.

APPENDIX A
DERIVATION OF THE CONFORMAL MAPPING, EQUATIONS (4) AND (5)

The derivation of the conformal mapping of the finned cylinder in Figure 2 onto a circle is divided into the following steps:

(1) Conformal transformation of the original figure in the z-plane onto the auxiliary plane z_1, in which the fins are mapped to arcs of a hyperbola (Figure 12):

$$z_1 = z + \frac{a^2}{z} \tag{A1}$$

Then, the points A through H and the corresponding points A_1 through H_1 in Figure 12 are given by

$$\begin{array}{ll}
A = +a & A_1 = +2a \\
B = -ae^{-i\theta} & B_1 = -2a\cos\theta \\
C = -be^{-i\theta} & C_1 = -(b + \frac{a^2}{b})\cos\theta + i(b - \frac{a^2}{b})\sin\theta \\
D = B & D_1 = B_1 \\
E = -a & E_1 = -2a \\
F = -ae^{i\theta} & F_1 = B_1 \\
G = -be^{i\theta} & G_1 = -(b + \frac{a^2}{b})\cos\theta - i(b - \frac{a^2}{b})\sin\theta \\
H = F & H_1 = B_1
\end{array} \tag{A2}$$

The lengths k and ℓ are

$$k = \frac{1}{4i}(C_1 - G_1) = \frac{1}{2}(b - \frac{a^2}{b})\sin\theta \tag{A3}$$

$$\ell = D_1 - \frac{1}{2}(C_1 + G_1) = \frac{1}{b}(b - a)^2\cos\theta \tag{A4}$$

The hyperbolic arc $C_1B_1G_1$ is now approximated by the circular arc through these points with the radius

$$R = \frac{1}{2\ell}(4k^2 + \ell^2) \tag{A5}$$

(2) According to Betz[23] this circular arc can be mapped onto a circle by means of

$$z_2 - \frac{k^2}{z_2} = z_1 + (b + \frac{a^2}{b})\cos\theta \tag{A6}$$

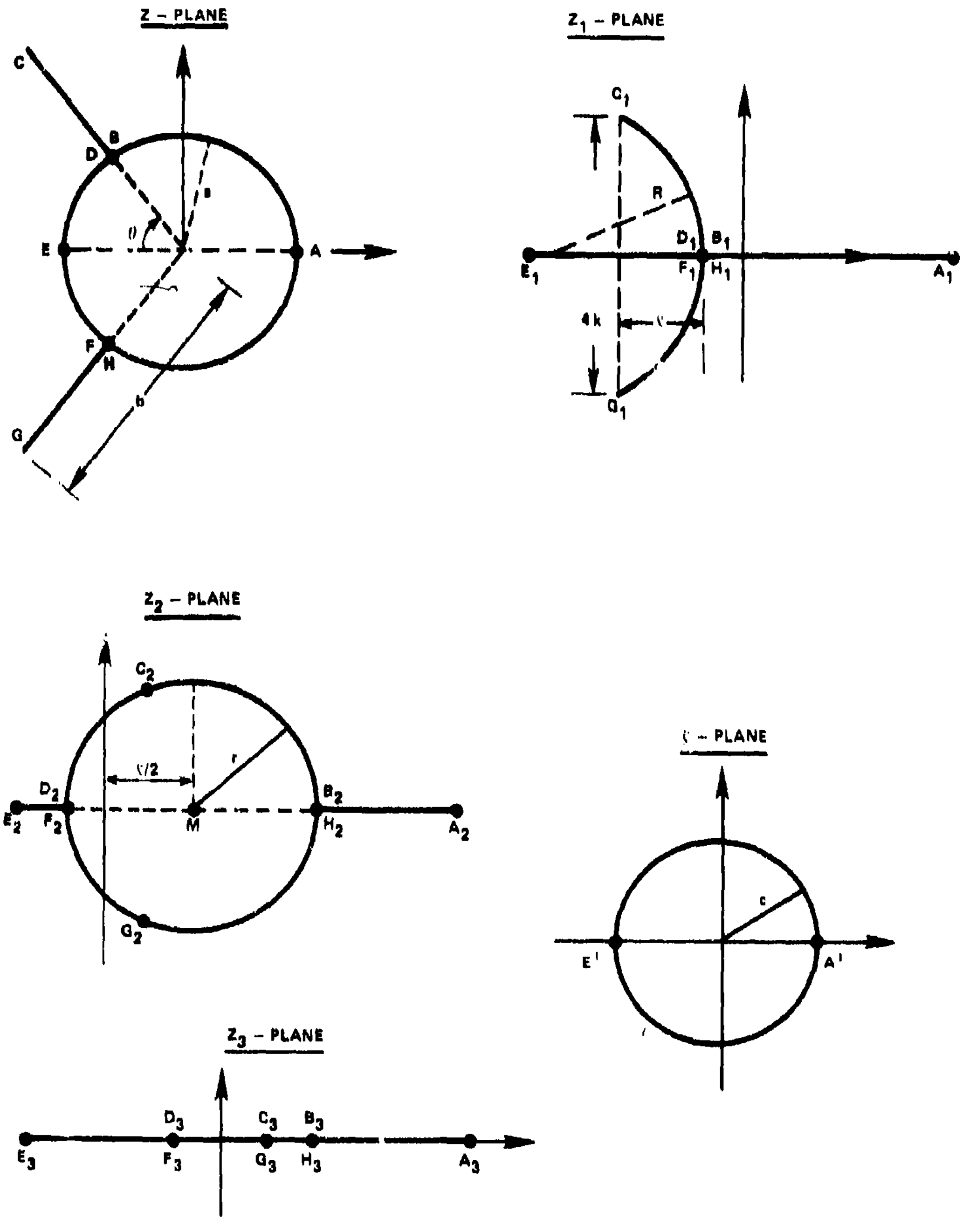

Figure 12 - Sequence of Conformal Mappings from a Circle with Two Dihedral Fins onto a Circle

with

$$A_2 = \text{positive root of } z_2 - \frac{k^2}{z_2} = 2a + (b + \frac{a^2}{b}) \cos\theta$$

$$B_2 = \frac{\ell}{2} + \frac{1}{2}\sqrt{4k^2 + \ell^2} = \frac{\ell}{2} + \sqrt{\frac{1}{2} R\,\ell} \tag{A7}$$

etc.,

where

$$M = \frac{1}{2}\ell \;, \quad r = \frac{1}{2}(B_2 - D_2) = \sqrt{\frac{1}{2} R\,\ell} \tag{A8}$$

(3) Now the figure in the z_2-plane is mapped onto a straight line in the z_3-plane by

$$z_3 = z_2 - \frac{\ell}{2} + \frac{r^2}{z_2 - \ell/2} \tag{A9}$$

All points of the figure lie on the real axis with

$$A_3 = A_2 - \frac{\ell}{2} + \frac{r^2}{A_2 - \ell/2}$$

$$B_3 = B_2 - \frac{\ell}{2} + \frac{r^2}{B_2 - \ell/2} = \sqrt{2 R\,\ell} \tag{A10}$$

etc.

(4) Finally, the straight line in the z_3-plane is mapped onto the circle in the ζ-plane with radius c by

$$\zeta + \frac{c^2}{\zeta} = z_3 - s \tag{A11}$$

with

$$s = \frac{1}{2}(A_3 + E_3) \tag{A12}$$

$$c = \frac{1}{4}(A_3 - E_3) \tag{A13}$$

(See Figure 12.) Combining the four transformations to two, one arrives at Equations (4) and (5).

APPENDIX B
LAURENT SERIES FOR w_R

The conformal mapping $z = f(\zeta)$ is expressed in an infinite series of the form

$$z = \sum_{q=-1}^{\infty} a_q \left(\frac{c}{\zeta}\right)^q , \quad \text{where } a_{-1} = c \tag{B1}$$

The principal part of $z\bar{z}$ on the circle σ (see Equation (13)), which is required to obtain $B_1(\zeta)$, is

$$\text{P.P.}(z\bar{z}) = \sum_{q=1}^{\infty} b_q \left(\frac{c}{\sigma}\right)^q \quad \text{on } |\zeta| = c \tag{B2}$$

Since it is very laborious to determine a_q and b_q analytically, these coefficients are computed numerically. From Equation (B1) it follows that on the circle

$$z = \sum_{q=-1}^{\infty} a_q \, e^{-iq\theta} \tag{B3}$$

where $\zeta = ce^{i\theta}$. Equation (B3) is a Fourier series whose coefficients can be determined from

$$a_q = \frac{1}{2\pi} \int_0^{2\pi} z \, e^{iq\theta} \, d\theta \tag{B4}$$

or in discretized form from

$$a_q \approx \frac{\Delta\theta}{2\pi} \sum_{\ell=1}^{N} z_\ell \, e^{iq\theta_\ell} \tag{B5}$$

The coefficients a_q are real if

$$z(0) = \overline{z(2\pi-\theta)} \tag{B6}$$

because

$$\begin{aligned} a_q &= \frac{1}{2\pi} \left[\int_0^{\pi} z \, e^{iq\theta} d\theta + \int_{\pi}^{2\pi} z \, e^{iq\theta} \, d\theta \right] \\ &= \frac{1}{2\pi} \int_0^{\pi} (z \, e^{iq\theta} + \bar{z} \, e^{-iq\theta}) d\theta \\ &= \frac{1}{\pi} \int_0^{\pi} \text{Re}(z e^{iq\theta}) d\theta \end{aligned} \tag{B7}$$

Similarly, Equation (B2) becomes on the circle

$$\text{P.P.}(z\bar{z}) = \sum_{q=1}^{\infty} b_q e^{-iq\theta} \tag{B8}$$

whose coefficients b_q are

$$b_q = \frac{1}{2\pi}\int_0^{2\pi} z\bar{z}\ e^{iq\theta}\ d\theta \tag{B9}$$

$$\approx \frac{\Delta\theta}{2\pi}\sum_{\ell=1}^{N} z_\ell \bar{z}_\ell\ e^{iq\theta_\ell}$$

Again, for the symmetry condition (B6) it can be shown in a way analogous to Equation (B7) that b_q is real.

As an example, for a circular cylinder with two fins (n=2) and various ratios a/b the coefficients a_q and b_q are displayed in Tables 1 and 2 for q=1 through 50 with $\Delta\theta = 2\pi/1080$. For $a/b = 0$, $a_q = b_q = 0$ except $a_1 = 0.25$, $b_1 = c^4 = 0.0625$. For the other extremum $a/b = 1$, $z = \zeta$ and thus all coefficients are zero. Despite the fineness of $\Delta\theta$ the data in both tables are accurate only to $\pm 5-06$ because of round-off errors.

TABLE 1 - COEFFICIENTS a_q FOR n = 2,
a:b = 0.2, 0.4, 0.6, 0.8

u_q	0.2	0.4	0.6	0.8
1	.2215E+00	.1521E+00	.7529E-01	.1976E-01
3	.3277E-01	.7232E-01	.5861E-01	.1880E-01
5	-.2307E-01	-.3519E-02	.3285E-01	.1699E-01
7	.1211E-01	-.1786E-01	.9091E-02	.1449E-01
9	-.2711E-02	.2623E-02	-.6748E-02	.1153E-01
11	-.3192E-02	.8739E-02	-.3884E-02	.8385E-02
13	.5080E-02	-.2165E-02	-.4524E-02	.5718E-02
15	-.3816E-02	-.5289E-02	.1864E-02	.2570E-02
17	.1091E-02	.1871E-02	.4813E-02	.3250E-03
19	.1364E-02	.3847E-02	.3255E-02	-.1299E-02
21	-.2452E-02	-.1857E-02	-.3664E-03	-.2263E-02
23	.1997E-02	-.2519E-02	-.2798E-02	-.2604E-02
25	-.6021E-03	.1490E-02	-.2477E-02	-.2422E-02
27	-.8119E-03	.1849E-02	-.2069E-03	-.1862E-02
29	.1510E-02	-.1363E-02	.1713E-02	-.1092E-02
31	-.1267E-02	-.1383E-02	.1947E-02	-.2760E-03
33	.3830E-03	.1236E-02	.5683E-03	.4442E-03
35	.5610E-03	.1042E-02	-.1041E-02	.9655E-03
37	-.1050E-02	-.1133E-02	-.1547E-02	.1233E-02
39	.8900E-03	-.7840E-03	-.7109E-03	.1240E-02
41	-.2641E-03	.1042E-02	.5904E-03	.1025E-02
43	-.4218E-03	.5828E-03	.1226E-02	.6546E-03
45	.7845E-03	-.9589E-03	.7647E-03	.2152E-03
47	-.6663E-03	-.4229E-03	-.2736E-03	-.2078E-03
49	.1916E-03	.8810E-03	-.9594E-03	-.5422E-03

TABLE 2 - COEFFICIENTS b_q FOR $n = 2$,

$a:b = 0.2, 0.4, 0.6, 0.8$

b_q	0.2	0.4	0.6	0.8
2	.6374E-01	.5487E-01	.3226E-01	.9395E-02
4	.3628E-02	.1867E-01	.2254E-01	.8742E-02
6	-.3233E-02	-.3536E-02	.1064E-01	.7721E-02
8	.2236E-02	-.3463E-02	.1438E-02	.6428E-02
10	-.1117E-02	.1407E-02	-.3201E-02	.4978E-02
12	.1626E-03	.1666E-02	-.3275E-02	.3495E-02
14	.4263E-03	-.1255E-02	-.9691E-03	.2099E-02
16	-.5955E-03	-.8888E-03	.1171E-02	.8869E-03
18	.4340E-03	.9275E-03	.1704E-02	-.6105E-04
20	-.1202E-03	.5127E-03	.7705E-03	-.7142E-03
22	-.1604E-03	-.7200E-03	-.5047E-03	-.1006E-02
24	.2676E-03	-.3047E-03	-.1055E-02	-.1145E-02
26	-.2397E-03	.5794E-03	-.6443E-03	-.1007E-02
28	.8122E-04	.1776E-03	.1910E-03	-.7229E-03
30	.6527E-04	-.4775E-03	.7025E-03	-.3690E-03
32	-.1744E-03	-.4507E-04	.5483E-03	-.1692E-04
34	.1556E-03	.3994E-03	-.2379E-04	.2753E-03
36	-.5747E-04	.3873E-04	-.4793E-03	.4691E-03
38	-.5401E-04	-.3344E-03	-.4689E-03	.5477E-03
40	.1143E-03	.8523E-06	-.7358E-04	.5157E-03
42	-.1106E-03	.2894E-03	.3247E-03	.3952E-03
44	.4343E-04	-.2913E-04	.5986E-03	.2197E-03
46	.3602E-04	-.2467E-03	.1314E-03	.2753E-04
48	-.8744E-04	.4166E-04	-.2114E-03	-.1453E-03
50	.8351E-04	.2113E-03	-.3357E-03	-.2706E-03

REFERENCES

1. Fink, P.T. and W.K. Soh, "Calculation of Vortex Sheets in Unsteady Flow and Applications in Ship Hydrodynamics." Tenth Symposium on Naval Hydrodynamics, 1974, 463.

2. Saffman, P.G. and G.R. Baker, "Vortex Interactions." Ann. Rev. Fluid Mech. 11 (1979), 95.

3. Clements, R.R. and D.J. Maull, "The representation of sheets of vorticity by discrete vortices." Prog. Aerospace Sci. 16 (1975), 129.

4. Kato, N., "Numerical Study on Transient and Quasi-steady Separated Flows Behind a Flat Plate and a Circular Cylinder by Potential Vortex Models." Ph.D.-Dissertation, Dept. of Naval Architecture, University of Tokyo, Nov. 1979.

5. Leonard, A., "Vortex Methods for Flow Simulation." To be published in Journal Comp. Phys.

6. Dawson, C.W. and J.S. Dean, "CMAP: A Program to Conformally Map the Unit Circle onto a Simple Closed Curve." Computation, Mathematics, and Logistics Department, David W. Taylor Naval Ship Research and Development Center. Unpublished computer program, 1971.

7. Grassmann, E., "Numerical Experiments with a Method of Successive Approximation for Conformal Mapping." Zeitschrift für Angewandte Mathematik und Physik 30 (1979), 873.

8. Chakravarthy, S. and D. Anderson, "Numerical Conformal Mapping." Mathematics of Computation 33 (1979), 953.

9. Mendenhall, M.R., S.B. Spangler, and S.C. Perkins, "Vortex Shedding from Circular and Noncircular Bodies at High Angles of Attack." Journ. AIAA, No. 79-0026, 1979.

10. Golovkin, V.A. and M.A. Golovkin, "Numerical solution for unsteady separated inviscid incompressible flow past an arbitrary body." Sixth Intern. Conf. on Numerical Methods in Fluid Dynamics. Lecture Notes in Physics, No. 90, Springer-Verlag, 1979, 253.

11. Miles, J.W., "On Interference Factors for Finned Bodies." Journ. Aero. Sci. 19 (1952), 287.

12. Bryson, A.E., "Evaluation of the Inertia Coefficients of the Cross Section of a Slender Body." Journ. Aer. Sci. 21 (1954), 424.

13. Milne-Thomson, L.M., "Theoretical Hydrodynamics." The MacMillan Co., New York, Fifth edition, 1968.

14. Prandtl, L., "Über die Entstehung von Wirbeln in der idealen Flüssigkeit." Vorträge aus dem Gebiet der Hydro- und Aerodynamik, Innsbruck, 1922, Berlin, 1924.

15. Wedemeyer, E., "Ausbildung eines Wirbelpaares an den Kanten einer Platte." Ingenieur-Archiv 30 (1961), 187.

16. Blendermann, W., "Der Spiralwirbel am translatorisch bewegten Kreisbogenprofil." Schiffstechnik 16 (1969), 3.

17. Pullin, D.I., "The large-scale structure of unsteady self-similar rolled-up vortex sheets." Journ. Fluid Mech. 88 (1978), 401.

18. Shoaff, R.L., "A Discrete Vortex Analysis of Flow About Stationary and Transversely Oscillating Circular Cylinders." Ph.D. Thesis, Naval Postgraduate School, Monterey, California, Dec. 1978.

19. Moore, D.W. and P.G. Saffman, "Axial flow in laminar trailing vortices." Proc. Roy. Soc. London A 333 (1973), 491.

20. Belotserkovskii, S.M. and M.I. Nisht, "Investigation of Special Features of Flow Over a Flat Plate at Large Angles of Attack." Fluid Dynamics 8 (1973), 772.

21. Lugt, H.J. and H.J. Haussling, "The Acceleration of Thin Cylindrical Bodies in a Viscous Fluid." ASME Journ. Appl. Mechanics 100 (1978), 1.

22. Sarpkaya, T., "An inviscid model of two-dimensional vortex shedding for transient and asymptotically steady separated flow over an inclined plate." Journ. Fluid Mech. 68 (1975), 109.

23. Betz, A., "Konforme Abbildung." Springer-Verlag, 2. Aufl. 1964.

INITIAL DISTRIBUTION

Copies	
1	APG 1 Lib
2	CHONR 1 Code 102/R. Lundegard 1 Code 430/J.C.T. Pool
2	USNA 1 Dept. Mech. Engr/ R.A. Granger 1 Lib
2	NAVPGSCOL 1 T. Sarpkaya 1 Lib
1	NAVWARCOL
1	USNROTC, ADM MIT
1	NCSC 1 D.E. Humphreys
1	NSWC, White Oak/Lib
1	NSWC, Dahlgren/Lib
4	NAVSEA 1 SEA 03C/J. Huth 1 SEA 03R1/J. Schuler 1 SEA 3212/W. Sandberg 1 SEA 63R3/T. Pierce
1	NAVAIR/440, W. Volz
1	NAVSHIPYD BREM/Lib
1	NAVSHIPYD CHASN/Lib
1	NAVSHIPYD MARE/Lib
1	NAVSHIPYD NORVA/Lib
1	NAVSHIPYD PEARL/Lib
1	NAVSHIPYD PTSMH/Lib
12	DTIC

Copies	
2	AFFDL 1 A. Fiore 1 W. Hankey
1	NASA Headquarters 1 EM-7/R. Dressler
3	NASA AMES 1 T. Leonard 1 U. Mehta 1 Lib
2	NASA Langley 1 D. Bushnell 1 Lib
1	U. of California/Dept Naval Arch 1 J.V. Wehausen
1	U. of Cincinnati/K. Ghia
1	Harvard U./Dept of Math 1 G. Birkhoff
1	Johns Hopkins U., APL/V. O'Brien
1	Iowa Inst. of Hydraulic Res. 1 L. Landweber
1	Hydronautics, Inc. 7210 Pindell School Road Laurel, MD 20810 1 M. Tulin
1	Nielsen Engineering & Res. Inc. Mountain View, CA 94043
1	Scientific Res. Associates, Inc. P.O. Box 498 Glastonbury, CT 06033 1 S.J. Shamroth

CENTER DISTRIBUTION

Copies	Code	Name
1	012	R. Allen
1	012.2	B. Nakonechny
1	012.3	D. Jewell
1	1500	W. Morgan
1	1501	R. Shoaff
1	154	J. McCarthy
1	1544	R. Cumming
1	1552	T. Wang
1	156	G. Hagen
1	1564	J. Feldman
1	1600	H. Chaplin
1	1606	S. De los Santos
1	1800	G.H. Gleissner
25	1802.1	H.J. Lugt
1	1802.2	F.N. Frenkiel
2	1809.3	D. Harris
1	184	J.W. Schot
1	1843	H.J. Haussling
20	1843	J. Telste
1	1844	S.K. Dhir
1	1900	M. Sevik
1	1901	M. Strasberg
1	1960	D. Feit
10	5211.1	Reports Distribution
1	522.1	Unclassified Lib (C)
1	522.2	Unclassified Lib (A)

DTNSRDC ISSUES THREE TYPES OF REPORTS

1. DTNSRDC REPORTS, A FORMAL SERIES, CONTAIN INFORMATION OF PERMANENT TECHNICAL VALUE. THEY CARRY A CONSECUTIVE NUMERICAL IDENTIFICATION REGARDLESS OF THEIR CLASSIFICATION OR THE ORIGINATING DEPARTMENT.

2. DEPARTMENTAL REPORTS, A SEMIFORMAL SERIES, CONTAIN INFORMATION OF A PRELIMINARY, TEMPORARY, OR PROPRIETARY NATURE OR OF LIMITED INTEREST OR SIGNIFICANCE. THEY CARRY A DEPARTMENTAL ALPHANUMERICAL IDENTIFICATION.

3. TECHNICAL MEMORANDA, AN INFORMAL SERIES, CONTAIN TECHNICAL DOCUMENTATION OF LIMITED USE AND INTEREST. THEY ARE PRIMARILY WORKING PAPERS INTENDED FOR INTERNAL USE. THEY CARRY AN IDENTIFYING NUMBER WHICH INDICATES THEIR TYPE AND THE NUMERICAL CODE OF THE ORIGINATING DEPARTMENT. ANY DISTRIBUTION OUTSIDE DTNSRDC MUST BE APPROVED BY THE HEAD OF THE ORIGINATING DEPARTMENT ON A CASE-BY-CASE BASIS.